Spectral Quantum Efficiency Measurements on Cs-K-Sb Photocathodes for the Energy-Recovery Linac Test Facility bERLinPro

MASTERARBEIT

zur Erlangung des akademischen Grades
Master of Science (M. Sc.)
im Fach Physik

eingereicht an der
Mathematisch-Naturwissenschaftlichen Fakultät
Institut für Physik
Humboldt-Universität zu Berlin

von
Hans Kirschner

Betreuung:

1. *Prof. Dr. Andreas Jankowiak*
2. *Prof. Dr. Aleksandr Matveenko*

eingereicht am: *9. Januar 2017*

Contents

1 Introduction

For modern spectroscopy and surface science, synchrotron light sources are of great relevance, since they provide photon beams of constant high brightness and brilliance. Thus solid-state surface science, biology, life science, chemistry and physics use synchrotron light [1].

Present, the brilliance is limited in storage rings, whereas Linacs show better properties. The brilliance is the number of emitted photons per seconds, solid angle, area of the source. Different from a storage ring, in linear accelerators the electron beam generation defines the properties of the beam inside the accelerator. The initial beam parameters are eminent for future light sources like Energy Recovery Linacs (ERLs) and Free Electron Lasers (FELs), since they are driven by linear accelerators. The effort in the improvement of initial parameters like the normalized emittance pays off by synchrotron radiation of higher brilliance. To enhance the performance of future ERL, the demonstration facility bERLinPro, see fig. 1.1, is under construction at Helmholtz-Zentrum Berlin [2]. Its main goal is to demonstrate the viability of an ERL planned for high average currents of 100 mA with maximum beam energies of 50 MeV and bunch lengths lower than 2 ps. A normalized emittance below 1 mm mrad is planned, to be competitive to new different synchrotron light sources.

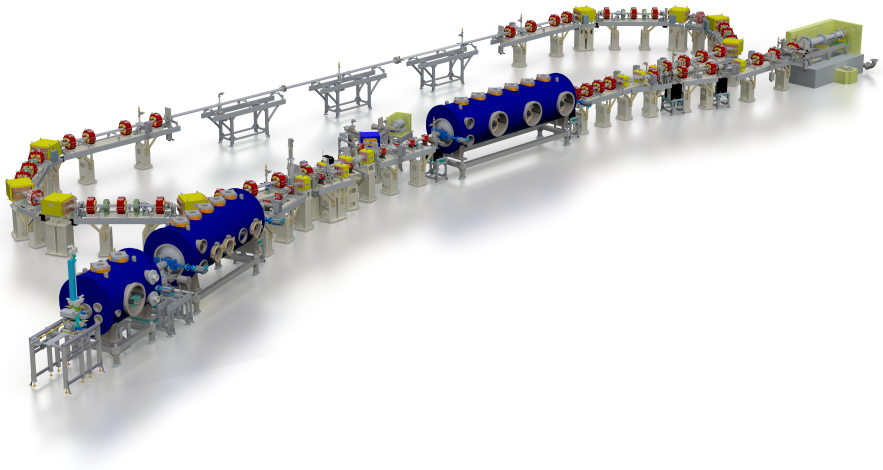

Figure 1.1: 3D model of the basic machine layout of bERLin Pro [3].

In order to reach the required parameters and to improve the beam quality, a superconducting radio-frequency photo electron gun (SRF photogun) was designed and built. This SRF photogun consists basically out of a photocathode, generating electrons by a laser beam via photoemission, which then are accelerated by a superconducting cavity and guided through a superconducting solenoid. The generation of electron sources will first be tested with Cu cathodes because of their better handling and robustness. In a second step, this type of cathode will be exchanged with Cs-K-Sb cathodes, providing higher quantum efficiencies of one magnitude and therefore higher average currents than Cu cathodes in the visible spectrum.

The growth of Sb, K and Cs in order to prepare Cs-K-Sb cathodes is demanding and requests an ultra-high vacuum. Even marginal changes to this process may influence the emittance, the lifetime and the spectral quantum efficiency of the

cathode and hence change the characteristics of the electron bunch in the SRF gun. In order to better understand and to optimize the preparation process, measuring the mentioned properties of the cathode is necessary.

This master thesis deals with the commissioning of an experimental setup, which is able to measure the spectral quantum efficiency (spectral QE) of a cathode in a wavelength range $\lambda = [400, 700]\,\mathrm{nm}$ and its time dependence at a fixed wavelength. The measurement of the intrinsic emittance of the cathode is done with a momentatron, as described in [4].

In chapter 2, an overview on the test-facility for the SRF photogun, called "GunLab", is given. The Spicer model [5] is introduced to explain the photoemission in three steps and to derive the spectral quantum efficiency for semiconductors. Further, the use of Cs-K-Sb cathodes is motivated by a comparison to other possible cathode materials. Chapter 3 describes the experimental setup and explains how the spectral quantum efficiency is calculated by measuring the spectral photocurrent and the spectral power of the light source. The commissioning of this setup is specified in the following chapter 4. Since the preparation of Cs-K-Sb is complex, the growth process and its monitoring is explained in chapter 5.

The last two chapters are dedicated to the results and their interpretation. Chapter 6 presents the spectral quantum efficiencies for five different Cs-K-Sb cathodes, prepared with different growth processes. For two of these cathodes also the lifetime was monitored and a mapping of the quantum efficiency at $\lambda = 515\,\mathrm{nm}$ was measured. Since the cathode will be used in a cryogenic environment, the behaviour of cold temperatures on the cathode and its quantum efficiency was recorded for one cathode. The interpretation of the data follows in chapter 7. A simplification of the used Spicer model by series expansion is presented, in order to extract two or as well one work function from fitting the spectral quantum efficiency. These work functions then are correlated with the quantum efficiency at $\lambda = 515\,\mathrm{nm}$ and the associated measuring time.

2 SRF-Photoinjector and the Spectral Quantum Efficiency

2.1 SRF-Photoinjector

A superconducting radiofrequency photoelectron injector (SRF photoinjector) for bERLinPro is tested in the compact test facility GunLab. These injectors are electron sources, promising high average current and short pulse duration for FELs or ERLs with high brightness electron beams. In order to characterize the beam parameters and the photocathode, a compact diagnostics beamline was designed, see fig. 2.1. The diagnostics beamline consists of:

- emittance scanner, in order to measure the emittance of the beam
- transverse deflecting cavity (TCAV) to measure the longitudinal phase space and the slice emittance
- spectrometer dipole for longitudinal phase space mapping
- Farady cup to measure the charge

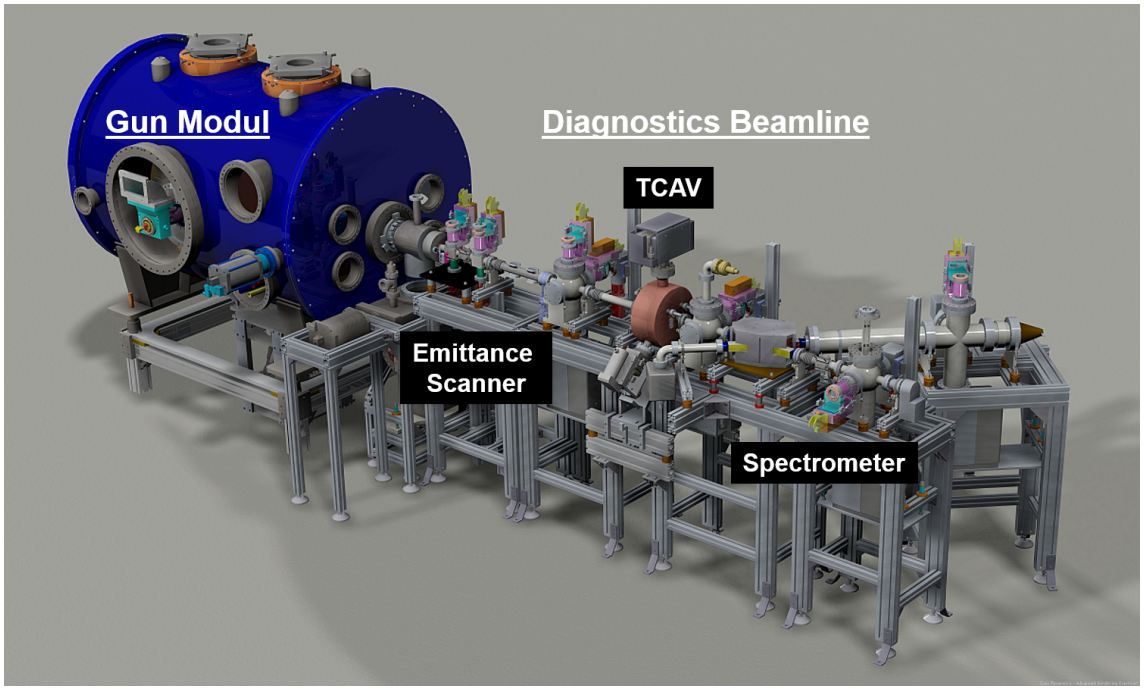

Figure 2.1: 3D model of GunLab, including the gun modul (blue vessel) and the diagnostics beamline with an emittance scanner, a transverse deflecting cavity (TCAV) and a spectrometer dipole for longitudinal phase mapping.

Basically, the SRF photoinjector consists out of a photocathode, a superconducting (SC) gun cavity, and an SC solenoid. A cross section of the gun is shown in fig. 2.2. The photocathode is irradiated by a laser beam inducing the photoelectric effect, in order to generate electrons, which are accelerated by the SC gun cavity, while the SC solenoid focuses their path.

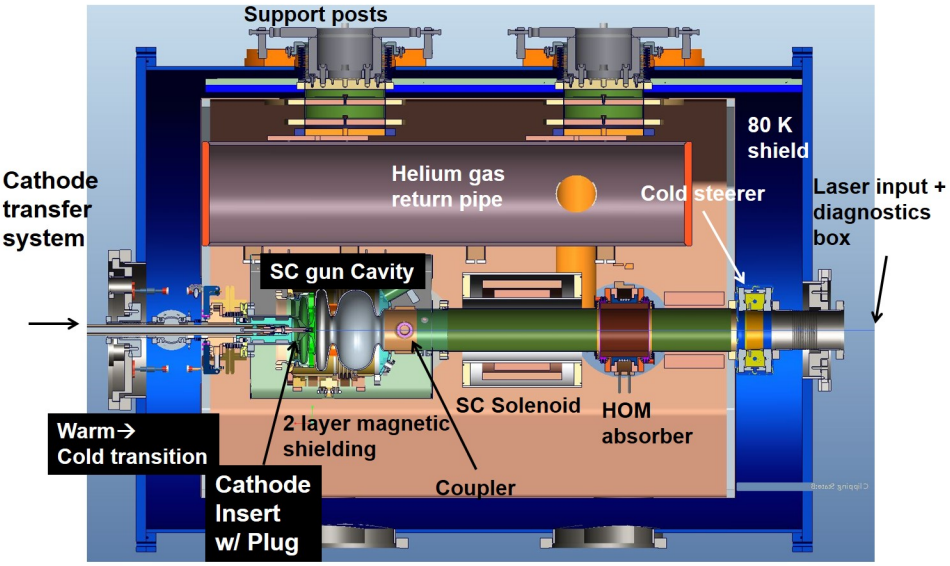

Figure 2.2: Cross section of the superconducting (SC) radio frequency photoinjector for bERLinPro. The laser beam enters the gun cavity and induces the photoelectrical effect on the photocathode. The electrons are accelerated by the SC gun cavity and focussed by the SC solenoid.

There are some challenges, concerning the use and the construction of an SRF photoinjector.
Working with high electric and magnetic fields, unfavorable effects occure, concerning the surface of the cavity. High external magnetic fields lead to a quench of the cavity with a negative effect on its superconductivity. Thus, the magnetic field, generated at the SC solenoid has to be shielded from the cavity with some effort. Further, multipacting can arise at already medium surface electric fields. High surface fields lead to field emission. These both effects occur at any high gradient accelerator cavity but are especially adverse at SRF photoinjectors, since the needed RF power for the cavity to reach a certain gradient increases. The generated heat increases the needed cooling and gives possibility for a quench of the cavity.

Since the SRF photoinjector works at cryogenic temperatures, the cavity has to be surrounded by liquid helium, followed by a vacuum, a magnetic shield, liquid nitrogen thermo shield and still another isolation vacuum. Designing and repairing this construction will need some additional effort.

Besides the SRF concept of a photoinjector, it is possible to use a DC-based concept, like at Cornell University [6]. There, a high-power injector was built using a DC photoemission gun, followed by a superconducting RF accelerating module. With a GaAs cathode, currents up to 52 mA were obtained. Using a CsK_2Sb cathode, a current up to 65 mA was reached. A current of 100 mA is required for the Cornell energy recovery linac prototype injector, which is the same value as planned for bERLinPro.

A robust photocathode of high quantum efficiency and long lifetime is necessary to ensure stable operation with a high average current, calculated by:

$$\overline{I} = f_{rep} \cdot q_b \tag{2.1}$$

Here f_{rep} is the repetition rate of the laser and q_b is the bunch charge, which mainly depends on the photocathode and the laser, since it is a function of the quantum efficiency QE, as well as the pulse energy E_{pulse} and the photon energy E_γ of the laser:

$$q_b = \frac{E_{pulse}}{E_\gamma} \cdot QE \cdot q_e \tag{2.2}$$

A charge of one electron is described by q_e. For GunLab, a bunch charge of $q_b = 77\,\mathrm{pC}$ is aimed.

The laser provides wavelengths of $\lambda = 257.5\,\mathrm{nm}$ for the use with a copper cathode and $\lambda = 515\,\mathrm{nm}$ ($E_\gamma \approx 2.4\,\mathrm{eV}$) for a Cs-K-Sb cathode. Further, it is possible to choose between several repetition rates in a range of $f_{rep} = [52\text{–}30\,000]\,\mathrm{Hz}$. Because of reasons of radiation protection, the repetition rate is limited to $f_{rep} < 10\,\mathrm{kHz}$ and the mean laser power has to be reduced by a factor of 1000. Further, because of transmission losses, just about half of the laser power will reach the cathode. For Cs-K-Sb photocathodes quantum efficiencies of about 5 % to 10 % are likely.

Using eq. 2.2, the needed pulse energy E_{pulse} then can be calculated via

$$E_{pulse} = \frac{E_\gamma}{QE \cdot \frac{1}{2} \cdot \frac{1}{1000}} \cdot \frac{q_b}{q_e}. \tag{2.3}$$

For a quantum efficiency of 5 % this results in a pulse energy of $E_{pulse} \approx 7.4\,\mu\mathrm{J}$, which fits with the following associated laser parameters of $\lambda = 515\,\mathrm{nm}$, $f_{rep} = 8\,\mathrm{kHz}$, $\overline{P}_{laser} = 60\,\mathrm{mW}$ and $\mathrm{FWHM}_{pulse} = 20\,\mathrm{ps}$. The emitted radiant power and energy are functions of the particular operational states. Especially the laser power may be change and reduced, in order to use photocathodes with quantum efficiencies up to 10 %.

2.2 The Spectral Quantum Efficiency

In 1958, a theory to describe the photoemission process was developed by Spicer [5]. Its main assumption is to consider the photoemission consisting out of three steps. The derived model is commonly employed to receive expressions like the quantum efficiency. Because of its importance for this study, the model and the derivation of the equation for the spectral quantum efficiency are described in the following sections. The goal is to extract the work function ϕ, which describes the minimum energy needed to remove an electron from a solid to the vacuum.

2.2.1 The Spicer Three Step Model

According to the Spicer three step model [7], the process of photoemission consists out of three independent steps, see also fig. 2.3a:

1. Excitation: By absorption of incident light with the energy $E_\gamma = h\nu$, an electron is excited from the initial state E_i to an excited state $E_i + h\nu$.

2. Transport: The electron moves through the crystal and in the best case towards the surface.

3. Escape: If the perpendicular momentum component is high enough to overcome the surface barrier, the excited electrons may leave the crystal.

The photoemission process is approximated by this model, which treats the excited electrons as single particles. Further it neglects quantum mechanic effects for electron ensembles. However, to obtain a model, which is able to provide analytical results, approximations are necessecary to be done. The density of states of a crystal and its band structure are represented by a rectangular shape.

Although the process of excitation, transport and escape may occur as well in metals, semiconductors have advantage over metals, concerning the quantum efficiency, see fig 2.3b. The step of the excitation works the same for both solids. The main difference lies in the transport, since semiconductors hold a bandgap. Electrons are excited to the conduction band. In the case of metals, it is likely for these electrons to hand over some energy to non-excited electrons, so both of them are excited but with an energy too low to pass the surface barrier. In contrast it is not allowed for excited electrons in semiconductors to hand over energy, since they would fall into the forbidden bandgap. These electrons stay in the so called "Magic Window" and contribute to the quantum efficiency by passing the surface.

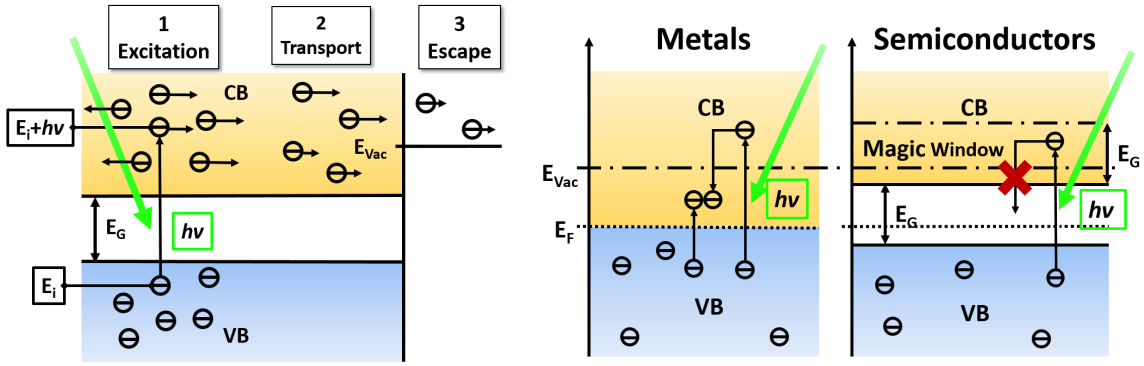

(a) (b)

Figure 2.3: The Spicer model and the advantage of semiconductors:
a) The three step model, in which the photoemission process is divided into three steps of excitation, transport and escape.
b) Difference of electron-electron scattering in metals and semiconductors. Regarding metals, an excited electron may loose its energy, necessary to escape, in a single electro-electron scattering event. With the "Magic Window", which semiconductors can have, it is possible for electrons to have enough energy to escape but not enough to produce pairs.
Abbreviations: conduction band (CB) and valence band (VB), gap energy (E_G), initial energy (E_i), energy of the incident light ($h\nu$), energy level of the vacuum (E_{Vac}), Fermi niveau (E_F).

2.2.2 The Spectral Quantum Efficiency for Semiconductors

The spectral quantum efficiency as a function of the photon energy can be derived by the Spicer model [5], beginning with the light intensity $I(x, h\nu)$ at a thickness x, after the incident light $I_0(h\nu)$ passes the surface of the solid:

$$I(x, h\nu) = I_0(h\nu)\,[1 - R(h\nu)]\,e^{-\alpha(h\nu)\cdot x} \tag{2.4}$$

Here $R(h\nu)$ is the reflectivity of the solids surface as a function of $h\nu$ and $\alpha(h\nu)$ is its absorption coefficient. For an infinitesimal thickness of the solid, the amount of absorbed light is given by the following differential equation:

$$\mathrm{d}I(x, h\nu) = I_0(h\nu)\,[1 - R(h\nu)]\,e^{-\alpha(h\nu)\cdot x}\alpha(h\nu)\,\mathrm{d}x \tag{2.5}$$

The electrons, excited by the light, may travel to the surface, escape and then contribute to the quantum efficiency at the given photon energy. This contribution $\mathrm{d}i(x)$ from a region of the solid of thickness $\mathrm{d}x$ at x is given by:

$$\mathrm{d}i(x) = P_{0\alpha}(h\nu, x, \mathrm{d}x) \cdot P_T(h\nu, x) \cdot P_E(h\nu) \tag{2.6}$$

Here $P_{0\alpha}$ is the probability for an electron to be excited above the vacuum level from a layer of thickness $\mathrm{d}x$, P_T is the probability for an excited electron to reach the surface of the solid with enough energy to escape and finally P_E is the probability for an electron to escape. $P_{0\alpha}$ and P_T can be written as:

$$\begin{aligned} P_{0\alpha}(h\nu, x, \mathrm{d}x) &= \alpha_{PE}(h\nu)I(x)\mathrm{d}x \\ &= \alpha_{PE}(h\nu)I_0(h\nu)\,[1 - R(h\nu)]\,e^{-\alpha(h\nu)\cdot x}\alpha(h\nu)\,\mathrm{d}x, \end{aligned} \tag{2.7}$$

$$P_T(x, h\nu) = \exp\left[-\frac{x}{L(h\nu)}\right] \tag{2.8}$$

Two new quantities are introduces with α_{PE} as the part of the electrons, excited above the vacuum level with the possibility to escape and $L(h\nu)$ as the scattering length.

Assuming a semi-infinite slab, this leads via $i(h\nu) = \int \mathrm{d}i(x)$ to:

$$\begin{aligned} i(h\nu) &= \int_0^\infty \alpha_{PE} I_0 \left[1 - R\right] e^{-\left(\alpha + \frac{1}{L}\right)\cdot x} P_E \, \mathrm{d}x, \\ i(h\nu) &= I_0 \left[1 - R\right] \frac{\alpha_{PE}}{\alpha + \frac{1}{L}} P_E \end{aligned} \tag{2.9}$$

In eq. 2.9 all quantities are functions of $h\nu$.

The quantum efficiency is defined as the amount of emitted electrons per absorbed photons. With the reciprocal of the absorption, called absorption length $l_\alpha = 1/\alpha$, it is possible to express the quantum efficiency in terms of the ratio of the absorption length to scattering length $\frac{l_\alpha}{L}$, the fraction of the above the vacuum level excited electrons $\frac{\alpha_{PE}}{\alpha}$ and the escape probability P_E, which leads to:

$$QE(h\nu) = \frac{N_e}{N_\gamma} = \frac{i}{I_0 \left[1 - R\right]} = \frac{\frac{\alpha_{PE}}{\alpha} P_E}{1 + \frac{l_\alpha}{L}} \tag{2.10}$$

In order to receive a preferably high quantum efficiency, it is necessary for the numerator and the denominator to reach values of 1, which means $\frac{\alpha_{PE}}{\alpha} \cdot P_E \to 1$ and $\frac{l_\alpha}{L} \to 0$.

Because of the magic window of semiconductors, see fig. 2.3b, electron-electron scattering is impeded, while electron-phonon scattering predominates. Electron-phonon scattering may place the electron in the right direction to escape, since it changes the direction of motion of the electron. By assuming a random walk process for the transport step with a sink at the surface of the crystal, the electrons may scatter many times with phonons, since the scattering process is nearly inelastic. More electrons are able to pass the surface barrier and P_E can be approximated to $P_E \approx 1$. Hence, just $\frac{\alpha_{PE}}{\alpha}$ as the ratio of electrons, excited above the vacuum level with the possibility to escpae, remains as nominator. Since all excited electrons are excited by $h\nu$ and the fraction of electrons with enough energy to pass the surface is given by $(h\nu - \phi)$, it is possible to write $\frac{\alpha_{PE}}{\alpha} = \frac{h\nu - \phi}{h\nu}$. Here, ϕ is the work function. Finally, the spectral quantum efficiency for semiconductors can be written as:

$$QE(\nu) = \frac{N_e}{N_\gamma} = \frac{1}{1 + \frac{l_a}{L}} \frac{h\nu - \phi}{h\nu} \tag{2.11}$$

2.3 Measuring the Quantum Efficiency and its Uncertainty

As aforementioned, the quantum efficiency is defined as the ration between the number of extracted electrons per incoming photons, both per second:

$$QE = \frac{N_e}{N_\gamma} \tag{2.12}$$

Rewriting the numbers N_e and N_γ in terms of $N_e = I/q_e$ and $N_\gamma = P_{Light}/E_\gamma$, it is possible to calculate the quantum efficiency with a measured current and power at a given wavelength via $E_\gamma = \frac{hc}{\lambda}$, using $hc = 1240\,\mathrm{eV\,nm}$, by the following formula written in practical units:

$$QE[\%] = \frac{I[\mathrm{A}]}{P_{Light}[\mathrm{W}]} \cdot \frac{1240\,\mathrm{eV\,nm}}{q_e \cdot \lambda\,[\mathrm{nm}]} \cdot 100[\%] \tag{2.13}$$

The uncertainty for the quantum efficiency is calculated by propagation of uncertainty, leading to the following equation:

$$\frac{u_{QE}}{QE} = \sqrt{\left(\frac{u_I}{I}\right)^2 + \left(\frac{u_P}{P}\right)^2 + \left(\frac{u_\lambda}{\lambda}\right)^2} \tag{2.14}$$

2.4 Cs-K-Sb Photocathodes

Depending on the material of the photocathode, different advantages and disadvantages arise. For the operation at bERLinpro and GunLab, a robust cathode is needed, providing a possibly high quantum efficiency at $E_\gamma = 2.4\,\mathrm{eV}$ ($\lambda = 515\,\mathrm{nm}$) of about $QE_{max} \sim 5\,\%$. In fig. 2.4 a comparison of the spectral quantum efficiencies for (multi-/bi-) alkali-antimonide cathodes, Cs-Te cathodes and cathodes of Cu and Pb are shown.

Cathodes made of metals are readily available and practically to handle. Their lifetime can almost be infinity, due to stability to residual gases and ion back bombardement. Further, metals provide a fast pulse response, allowing the generation of ultra-short bunches and pulse shaping in the fs region. A prominent example is copper. Additional to the mentioned properties of metal cathodes, copper provides a relatively high quantum efficiency and a good electrical and thermal conductivity. This type of cathode will be used in GunLab before the Cs-K-Sb cathodes, since the first experiments will be performance tests of the gun cavity with increasing RF-power. Therefore an easily available cathode is more practical, than a complex prepared Cs-K-Sb cathode. Disadvantages of metals are a comparatively low quantum efficiency and the laser power needs to induce the photoelectric effect in the UV region.

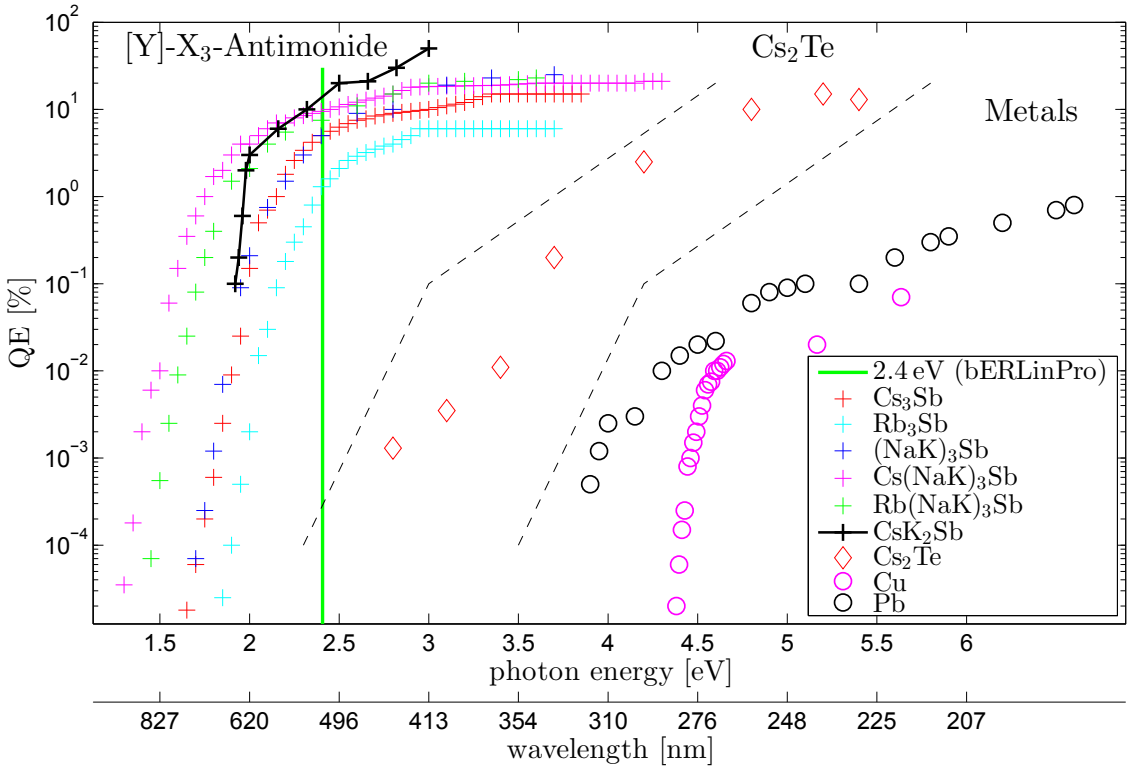

Figure 2.4: Spectral quantum efficiency for different materials. The green vertical line marks the photon energy $E_\gamma \approx 2.4\,\mathrm{eV}$, used at bERLinPro. The values are taken from [5, 8–11] for [Y]-X_3-Antimonide, CsK_2Sb, Cs_2Te, Cu and Pb.

Cathodes made of semiconductors are favorable, as the quantum efficiency is increased. Some of these cathodes are Ga-As, Cs-Te and Cs-K-Sb. All these cathodes provide several advantages and disadvantages. Besides a quantum efficiency of $\sim 10\,\%$ in the visible region, cathodes made of Ga-As are very reactive, therefore a vacuum $< 10^{-11}\,\mathrm{mbar}$ is necessary to prevent impurities, which would lead to a decrease in the quantum efficiency. Cathodes of Cs-Te provide high quantum efficiencies, but rather in the UV region. A Cs_2Te photocathode is used currently at FLASH [12], driven with a wavelength in the UV [9]. Especially antimony based cathodes provide high quantum efficiencies in the visible region.

In order to reach quantum efficiencies of $\gtrsim 5\,\%$ in the visible region, Cs-K-Sb photocathodes are suitable, since they provide the highest quantum efficieny at $E_\gamma = 2.4\,\mathrm{eV}$. Besides their advantage relating to the quantum efficiency, these cathodes place high demands on the preparation process and the subsequent handling. Research and development concerning the reproducibility of the preparation process, the (spectral) quantum efficiency and the lifetime of the photocathodes are necessary to enhance their viability.

3 Experimental Setup to Measure the Spectral Quantum Efficiency

An experimental setup was designed to measure the spectral quantum efficiency of a photocathode. The working principle is sketched in fig. 3.1. The main parts are a white light source, a monochromator, an optical path, described in the following sections, and the photocathode itself. In order to measure the power of the light, a calibrated photodiode is used. The photocurrent is measured with a biased pickup anode, combined with a pA-meter. This chapter was previously presented in the Forschungsbeleg by Hans Kirschner [13], except for some marginal changes.

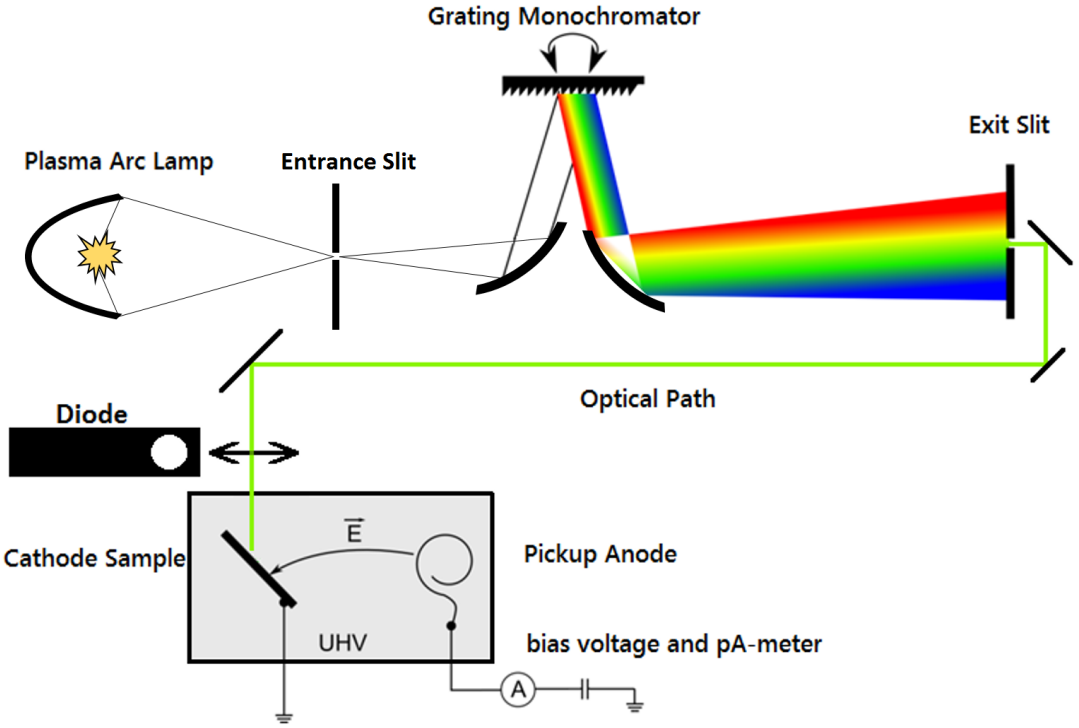

Figure 3.1: Scheme of the experimental setup, beginning with a white light source. The light is guided through a monochromator and afterwards through an optical path on the cathode, inducing the photoelectrical effect. The power of the monochrome light is measured by a diode. The electrons are measured via a pA-meter.

3.1 Plasma Arc Lamp

The plasma arc lamp "OBB PowerArc" by HORIBA Scientific is used as a white light source, since it offers high wattage power output over a broad wavelength range. Its specs are given in tab. 3.1.

parameter	value
lamp type	Xe arc lamp
lamp wattage	75 W
optical power	7.5 W
power supply stability after warm-up	0.2 %

Table 3.1: Specification of the white light source by HORIBA [14].

3.1.1 Lamp Housing

The housing design of the used lamp differs from typical designs in order to preserve as much power output as possible, see fig. 3.2. Unlike conventional designs, the OBB PowerArc works with an enveloping ellipsoidal reflector, that collects the light emitted by the lamp arc. The light is then focused to the second focal point outside of the lamp housing to enter the monochromator.

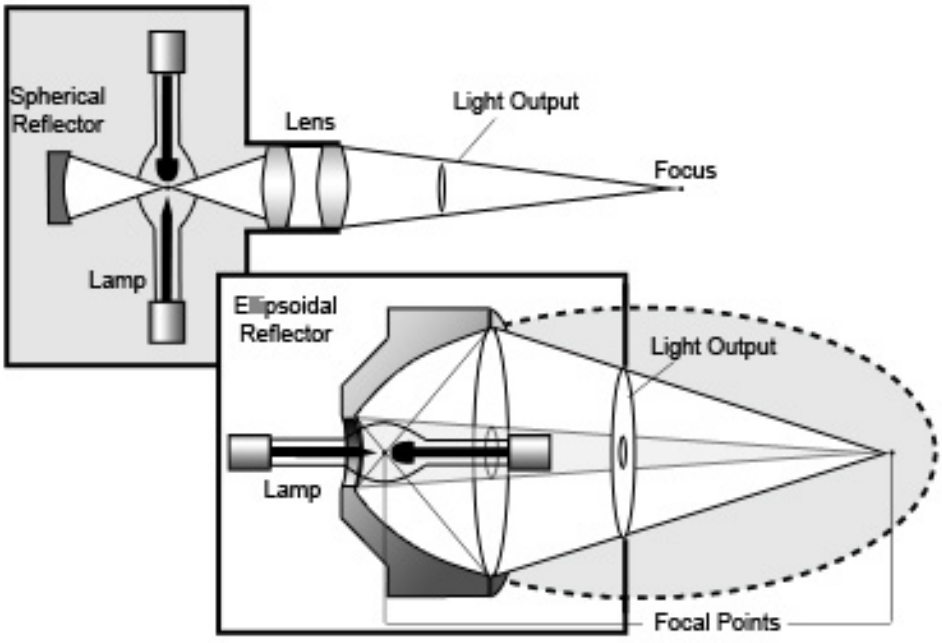

Figure 3.2: OBB PowerArc Xe arc lamp housing (foreground), using an ellipsoidal reflector, compared to a common housing (background) [15].

3.1.2 Xe Arc Lamp Spectrum

The spectral output of the used Xe arc lamp is shown in fig. 3.3. The related measuring range of $\lambda = [400, 700]$ nm for this study is marked.

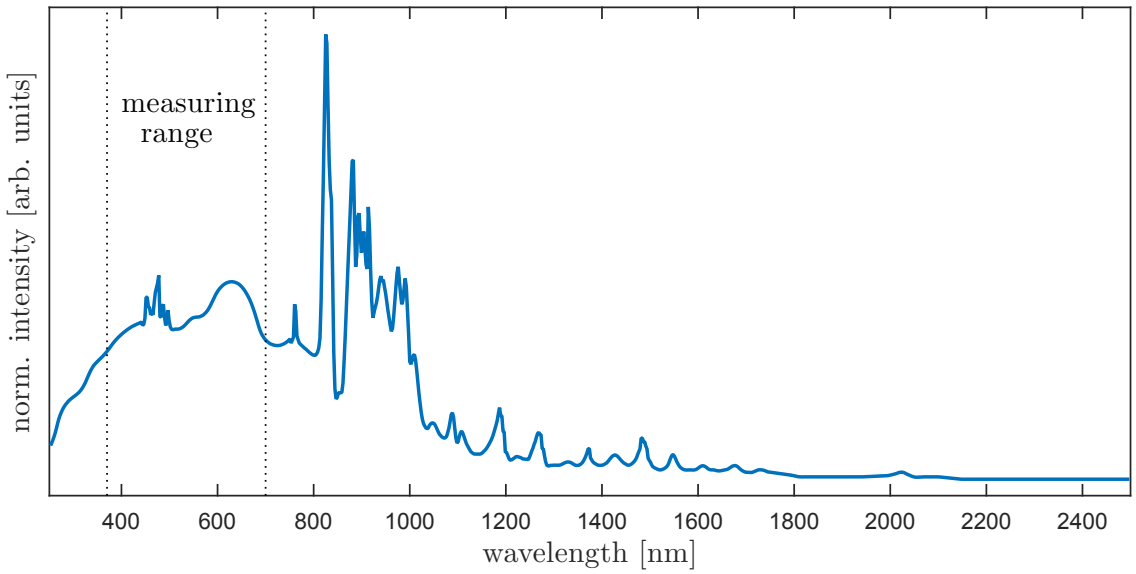

Figure 3.3: Xe arc lamp spectrum, data taken from [15].

3.2 Monochromator

In this setup a Czerny-Turner type monochromator by HORIBA Scientific is used. It features manual digital wavelength control with a wavelength display. An integrated motor can be controlled by a computer to operate the wavelength control by remote. For communication between the monochromator and the computer a Python[1] program was written. The parameter of the monochromator are given in tab. 3.2.

parameter	value
wavelength range	180 nm–1000 nm
throughput	≈ 60 % at 300 nm
accuracy	±0.25 nm (using motorizing option under computer control) ±1 nm (using manual wavelength control)

Table 3.2: Specs of the used monochromator at 1200 line/mm ruled grating [16].

Gratings

Inside the monochromator there are two gratings available in order to optimize the power output for different wavelength regions, see fig. 3.4. Since the operation wavelength of the laser at bERLinPro is going to be 515 nm, the 500 nm grating was chosen because of its maximum efficiency at ~ 500 nm.

[1] https://www.python.org/

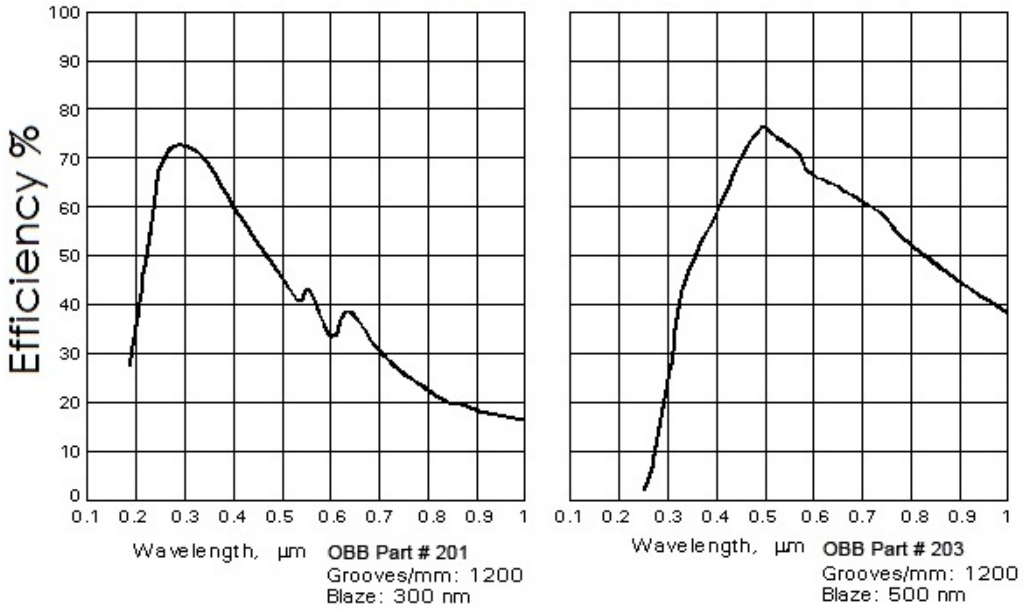

Figure 3.4: Grating efficiencies optimized for wavelengths around 300 nm and 500 nm [17].

3.3 Influence of the Band Width

The uncertainty of the wavelength is associated to its bandwidth. The monochromator does not provide a single wavelength. Integrating over several [nm] is necessary to obtain a required amount of power, since the optical setup provides a spectral flux in units of [W/nm]. This results in a band width around the adjusted wavelength. It is possible to manipulate the band width by the slit width of the entrance and exit slit. The band width can be calculated by

$$BW = \frac{W}{n \cdot L \cdot F} \tag{3.1}$$

where the order integer $n = 1$, the grating $L = 1200\,\text{lines/mm}$ and the focal length of the monochromator $F = 200\,\text{mm}$. The slit width W remains variable, resulting in $BW = BW(W)$ as a linear function in W. For a slit width of $W = 1.00\,\text{mm}$ the resolution of the monochromator is $BW = 4.17\,\text{nm}$. Going to smaller slit widths the resolution would improve, but the power output would decrease, which is unwanted. A band width of $BW \approx 4\,\text{nm}$ represents a reasonable compromise, leading to an uncertainty for λ of $u_\lambda = 2\,\text{nm}$. For $\lambda \in [400, 700]\,\text{nm}$ this results in a relative error of 0.5 % down to 0.25 %.

The measurement concerning the power output as a function of the band width is shown in sec. 4.6, see fig. 4.8.

3.4 Optical Path

The optical path is designed to image a light spot onto the cathode, as shown in fig. 3.5.

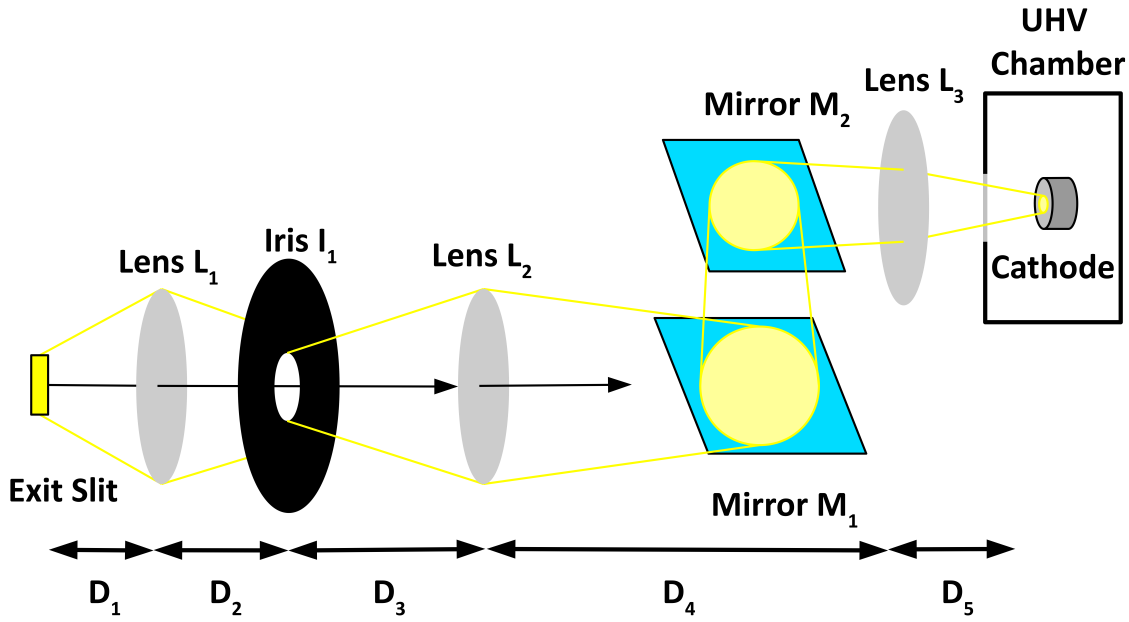

Figure 3.5: Sketch of the way, the light is going, from the exit slit of the monochromator to the cathode's surface.

At a distance of $D_1 = 75\,\text{mm}$ behind the exit slit of the monochromator a focussing lens L_1 with a focal length of $f_1 = 75\,\text{mm}$ was positioned to capture as much light as possible. Afterwards a setup of two lenses L_2 and L_3 images the iris aperture I_1 onto the cathode. The iris is intentional placed out of the focal point of L_1, since a light spot larger than the iris aperture is needed to retain the possibility of changing the spot size. The surface of the cathode serves as a screen for the imaged light spot. By changing the iris aperture, the spot size on the cathode changes as well. The distances between the optical components are shown in table 3.3a. The focal lengths of the lenses are shown in table 3.3b. Summed up, the total length is $D_{tot} \approx 1\,\text{m}$.

Path	Distance [mm]
D_1	~ 75
D_2	~ 30
D_3	~ 115
D_4	~ 625
D_5	~ 260
D_{tot}	~ 1105

(a)

Lens	Focal Length f [mm]
L_1	75
L_2	250
L_3	200

(b)

Table 3.3: a) Path distances D_i, b) Focal lengths of used lenses.

All values in tab. 3.3a are rounded. Calculating the D_5 by using D_1 to D_4 leads to D_5 = 262.7 mm and $M \approx 0.6$, which corresponds to the measured values. The magnification M is measured in sec. 4.5.

In fig. 3.6, the optical path from the iris to the cathode is plotted, showing the way of the light. Since the iris sits inside the focal length of the lense L_2, a virtual image is generated. This image then is guide through the lense L_3 onto the cathode. The magnification results in $M \sim 0.6$, which fits with the aforementioned calculation. For example, the minimal spot size of the iris of 0.8 mm is imaged onto the cathode with a smaller spot size of ~ 0.5 mm.

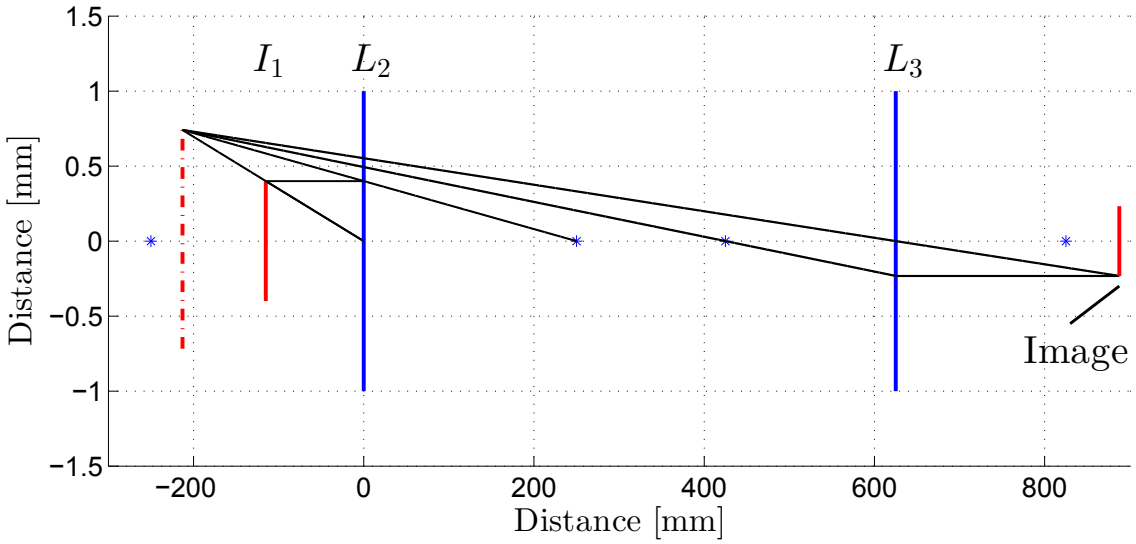

Figure 3.6: Optical path from the aperture of the iris to the cathode's surface, resulting in a magnification of $M \sim 0.6$. The lenses L_2 and L_3 correspond to those in tab. 3.3b. The stars * mark the focal length of the lenses.

3.5 Power Measurement

The power is measured with the power meter bundle PM130D from Thorlabs, figure 3.7. This bundle contains the digital power meter PM100D with the fitting diode S130C, gauged for a wavelength range of $[400, 1100]$ nm. Another diode is necessary, to measure in the UV region. The S130VC covers a wavelength range of $[200, 1100]$ nm. The **S130VC** was chosen because of the extended wavelength range. Table 3.4 shows the dedicated properties of both qualified diodes.

Figure 3.7: Digital Power Meter by Thorlabs with S130C sensor [18].

	S130VC	S130C
aperture size	ø 9.5 mm	
wavelength range	200–1100 nm	400–1100 nm
power range	500 pW–0.5 mW	500 pW–5 mW
(w/ integrated filter)	(Up to 50 mW)	(Up to 500 mW)
detector type	Si photodiode (UV Extended)	Si photodiode
measurement uncertainty	±3 %(440–980 nm) ±5 %(280–439 nm) ±7 %(200–279 nm, 981–1100 nm)	±3 %(440–980 nm) ±5 %(400–439 nm) ±7 %(981–1100 nm)

Table 3.4: Specification of photodiode power sensors from Thorlabs [19].

The error of the measured power is calculated by the following formula:

$$u_P = \sqrt{u_{system}^2 + u_{random}^2} \tag{3.2}$$

Here u_{system} is the error given by the system of photodiode and power meter and u_{random} is the statistical error, estimated by a sample of 100 measurements. The variation in the spectral power measured with the S130C approaches zero, which is why this error becomes insignificant. Only the systematic error remains as the significant part, given by the measurement uncertainty in table 3.4. Finally, u_P has a magnitude of 3 % or 5 % in a wavelength region [400, 700] nm.

3.6 Photocurrent Measurement

The photocurrent is measured with the pA-meter Keithley 6487/E with a bias voltage of $U_{bias} = 300\,\mathrm{V}$, whose accuracy is given by tab. 3.8a. The associated circuit diagram is shown in fig. 3.8b.

The error of the measured current is calculated in the same way as eq. 3.2. Since the statistical error in this case is estimated by a sample of just 20 measurements, it can not be neglected. The overall uncertainty of the current is of a magnitude $u_I \leq 0.5\,\%$.

Dark Current

The dark current I_D is the current, measured without light of the aforementioned light source falling on the cathode. However, a residual current may be measured by rest light inside the preparation chamber of the cathode. For example, it was of avail to turn of the mass spectrometer, since its filament emit light, when turned on. It is necessary to substract this current from the measured photo current to handle offset effects:

$$I_{photo} = |I_{meas} - I_D| \tag{3.3}$$

By using the absolute value, the photocurrent turns positive, which is more practical for further calculations. The magnitude of the dark current is $I_D \sim 1\,\mathrm{nA}$ and usually

range	accuracy		
2 nA	0.3 %	+	400 fA
20 nA	0.2 %	+	1 pA
200 nA	0.15 %	+	10 pA
2 µA	0.15 %	+	100 pA
20 µA	0.1 %	+	1 nA
200 µA	0.1 %	+	10 nA
2 mA	0.1 %	+	100 nA
20 mA	0.1 %	+	1 µA

(a)

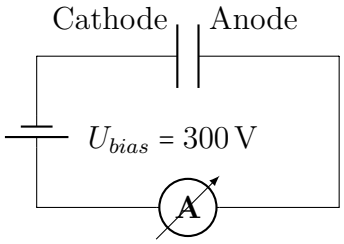

(b)

Figure 3.8: a) Accuracy of the Keithley 6487/E depending on the used range [20], b) Circuit diagramm, describing the measurement of the photocurrent.

at least one magnitude smaller than the measured current. Thereby the uncertainty of the photocurrent mainly depends on the uncertainty of the measured current.

$$u_{I_{photo}} = \sqrt{(u_{I_{meas}})^2 + (u_{I_D})^2} \tag{3.4}$$

3.7 Estimation of the Quantum Efficiencies Uncertainty

Via the measured photocurrent and the power of the light, the spectral quantum efficiency can be calculated by eq. 2.13. Its associated uncertainty can be calculated via eq. 2.14.

The main influence on the uncertainty of the quantum efficiency can be estimated by the maximum relative uncertainties of the single quantities, given in table 3.5

quantity	max. rel. uncertainty
power P	3 % – 5 %
current I	1 %
wavelength λ	0.5 %
quantum eff. QE	≈ 3 % – 5 %

Table 3.5: Summary of uncertainties and estimation of the overall uncertainty of the quantum efficiency.

Table 3.5 shows, that the uncertainty of the quantum efficiency mainly depends on the uncertainty of the power and therefore depending on the uncertainty of the measurement uncertainty of the photodiode power sensor.

4 Commissioning of the Experimental Setup

In order to ensure the reproducibility of the data recorded with the aforementioned experimental setup, it is necessary to characterize its properties like the spectral power output or the bandwidth of the light. This section deals with first measurements of the setup and its commissioning. The sections 4.1, 4.2, 4.3 and 4.4 have been published previously in [13], except for some marginal changes.

4.1 Measuring Routine

In order to measure the power and the photocurrent, a Python routine was written. The power P and the photocurrent I are measured seperately. Its particular range of application is explained below.

The Power

In the beginning, the motor of the monochromator and the power meter are opened as objects inside Python. Afterwards the monochromator motor is initialised to the mechanical zero, which is then associated with the current wavelength by manual input. The scanning range, as well as the step size are prompted. As step sizes only integer divisors are allowed. In this work a scanning range of $[400,\ 700]\,\mathrm{nm}$ with a step size of $\Delta\lambda = 5\,\mathrm{nm}$ is used as standard.

After the motor approaches the lower scanning range, the first measurement is executed. Each measurement consists of 100 single measurements, performed automatically by the PM130D using the current wavelength by reason of right calibration. From these 100 values the mean and the standard deviation are calculated. In order to receive the overall uncertainty, the root mean square of the standard deviation and the systematical error, given by table 3.4, is calculated by $u_{Power} = \sqrt{u_{stat}^2 + u_{sys}^2}$.

In the end the monochromator motor and the power meter are closed as objects.

The Photocurrent

The first part of this routine works similarly to the routine for measuring the power. Two objects are opened, both the monochromator motor and the pA-meter. The pA-meter is adjusted to supply a bias voltage of $U_{bias} = 300\,\mathrm{V}$, which may be changed. After the initialization of the motor, again the scanning range and the step size are prompted.

A measurement of the current consists of 20 single measurements, again performed automatically by the pA-meter. The aqcuisition takes about 7 s, representing a reasonable compromise concerning the measuring duration and the accuracy of the measurement. For example the aqcuisation of 100 single measurements would last about 35 s. The mean is as well queried from the pA-meter. Its overall uncertainty is calculated as for the power using the systematic uncertainties in tab. 3.8a.

In addition, the dark current I_D is aquired and substracted automatically from the photocurrent. Also its uncertainty is considered.

Finally, again the monochromator motor and the pA-meter are closed as objects.

The Software Concept

Both, the routine for measuring the power and the photocurrent are based on the same software concept, which is shown in fig. 4.1. First, it can be chosen between the photocurrent or the power. Afterwards, the routine opens the necessary devices. The measuring parameters have to be declared, before the actual scan starts. Finally, the measured values are saved and all opened devices are closed.

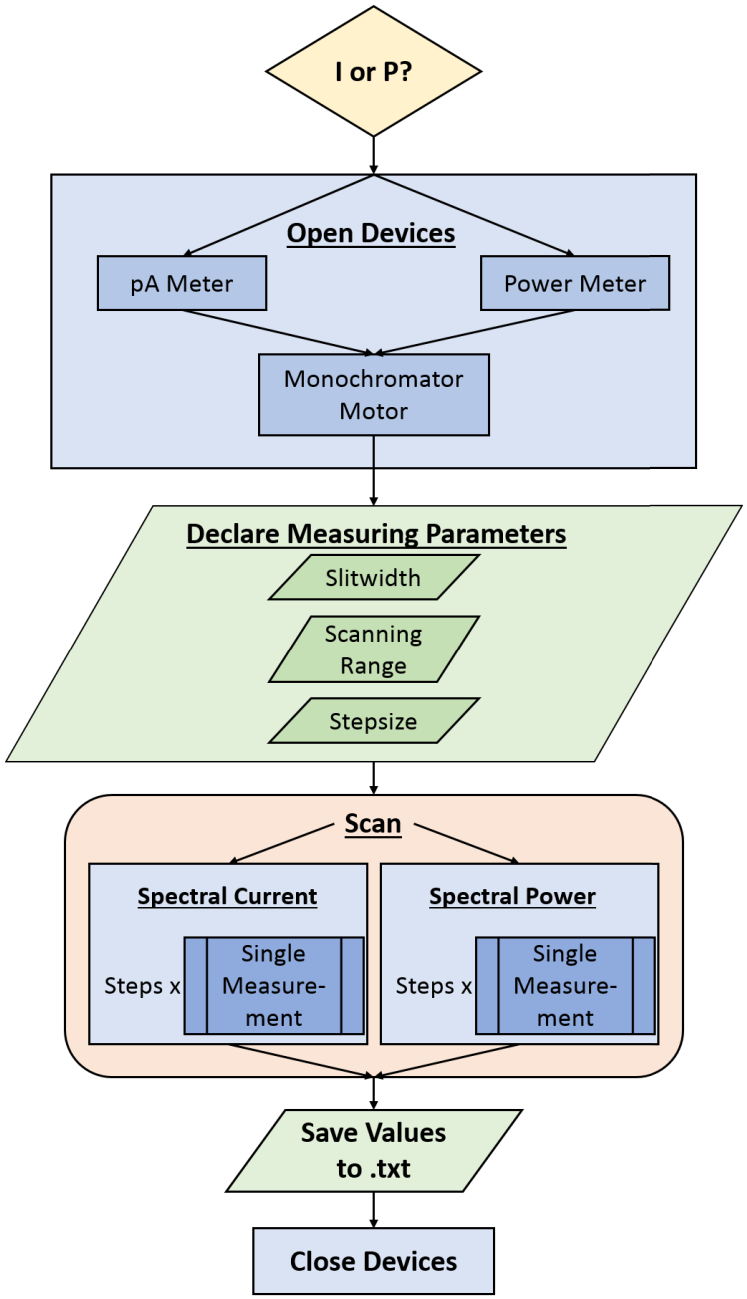

Figure 4.1: Flowchart of the software concept. Measuring the power P and the photocurrent I is based on the same concept.

4.2 Transmission Efficiency

The spectral power of the experimental setup depends on the power output of the Xe arc lamp, the grating inside the monochromator as well as the transmission of the components of the optical path, see fig. 3.5.

To enter the vacuum chamber with the photocathode inside, the light still has to pass a borosilicate viewport with a wavelength depending transmission, see fig. 4.2. This study uses a wavelength range of $[400, 700]\,\mathrm{nm}$. For wavelengths lower than 400 nm the power output of the experimental setup approaches zero. For wavelengths higher than 700 nm the measured quantum efficiency approaches zero. In this region a nearly constant transmission of ~ 93 % is prognosted for the viewport, see fig. 4.2b. In order to receive the spectral power of the whole experimental setup, another measurement including the viewport was executed. The result is shown in fig. 4.3. The spectral power decreases because of the influence of the viewport. As prognosted, the transmission is nearly constant of about 93 %.

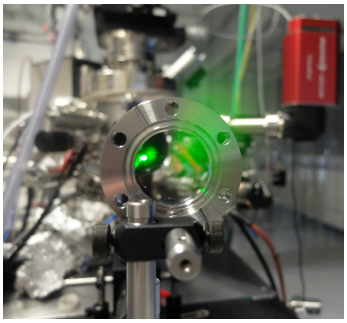

(a)

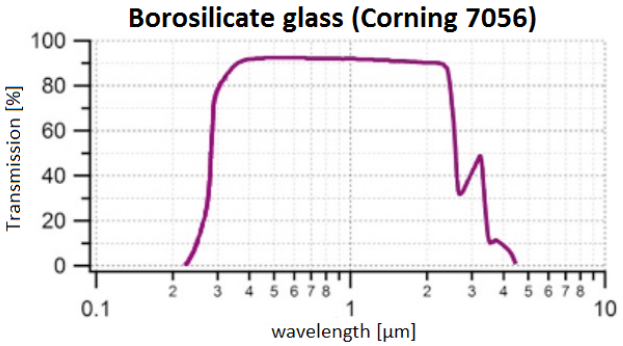

(b)

Figure 4.2: a) Borosilicate viewport VPCF16B-L, used as viewport to the UHV chamber,
b) and its transmission in a region of 100 nm to 10 µm [21].

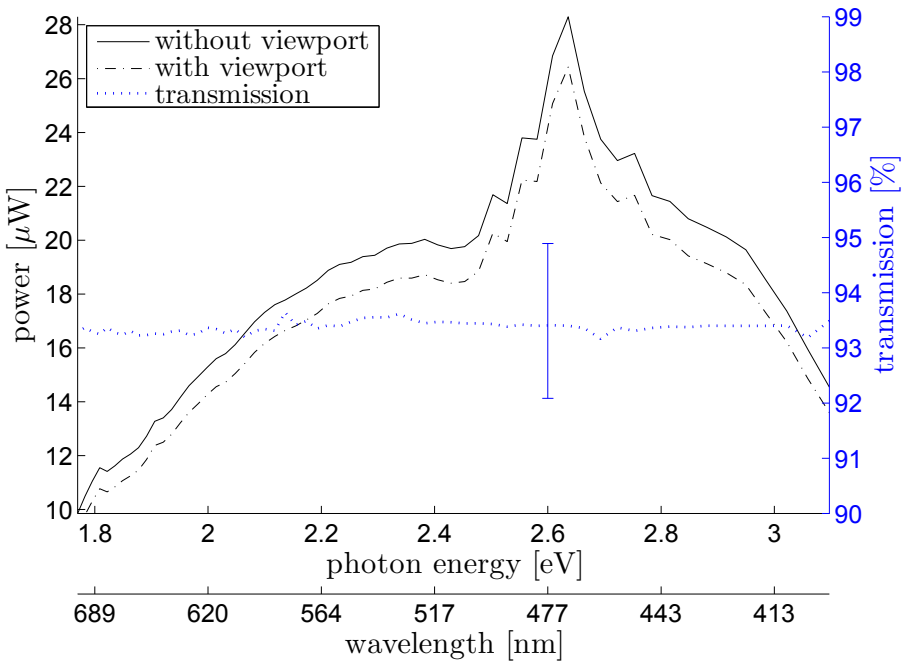

Figure 4.3: The transmission efficiency of the experimental setup, measured without and with viewport. Additional, the transmission of the viewport was plotted in blue. The errorbar at 2.6 eV indicates an error of 3 %.

Besides the transmission of the viewport, these plots show that the measurement of the power is working as planned. The associated errors are calculated.

4.3 Bias Voltage

When electrons are emitted without an impuls away from the emitting surface, they form a space charge in front of it. The field of this charge distribution screens the electrical field between cathode and anode, which leads to a loss of measured electrons. By increasing the bias voltage, the measured current rises, following the Child-Langmuir-Law for parallel diodes [22]:

$$I = \frac{4\epsilon_0}{9}\sqrt{\frac{2e}{m_e}}\frac{S}{d^2}\cdot U_{bias}^{3/2} \tag{4.1}$$

However, it is necessary to collect all electrons to make a confident statement about the photocurrent. As the bias voltage rises, a point will be reached, where all electrons are collected and the measured current is no longer affected by a change in U_{bias}. In fig. 4.4 the photocurrent was measured for different bias voltages. A plateau forms in the region $U_{bias} > 100\,\mathrm{V}$, which indicates, that no more charge carriers will add up by increasing the voltage. A bias voltage of 300 V ensures to be out of the space charge region. For a distance of cathode to anode of about $d_{CA} \approx 1\,\mathrm{mm}$, this resuts in an electrical field strength of $E_{CA} \approx 300\,\frac{\mathrm{V}}{\mathrm{mm}} = 0.3\,\frac{\mathrm{MV}}{\mathrm{m}}$.

These plots also show, that the measurement of the current is working as planned. Again, the associated errors are calculated.

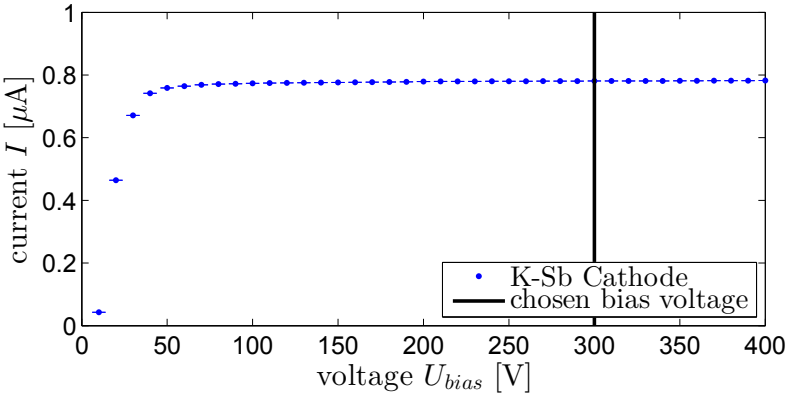

Figure 4.4: Photocurrent for different bias voltages U_{bias}; at $\lambda = 515\,\text{nm}$. The chosen bias voltage of $U_{bias} = 300\,\text{V}$ ensures to be out of the space charge region $< 70\,\text{V}$. For the used distance of cathode to anode of 1 mm, the voltage scale conforms to a field strength scale of [V/mm].

4.4 Filter for the Second Order

The Xe arc lamp is emitting in a large wavelength range from the UV region to the infrared region. The monochromator covers a mechanical scanning range of $[0, 1100]\,\text{nm}$. Scanning in $[400, 700]\,\text{nm}$, the second order of the monochromator becomes significant. Light of a wavelength $\lambda \leq 350\,\text{nm}$ induces the photoelectric effect inside the cathode for $\lambda \leq 700\,\text{nm}$ via its second order. This is an unwanted effect, since in this region the photocurrent should decrease because of lower photon energy. Therefore a Newport filter [23] with a cut-on wavelength of 345 nm ($\sim 3.6\,\text{eV}$) was integrated between the lamp and the monochromator. The result is shown in fig. 4.5.

Both measurements were take succesively, first without and then with a filter. The increase in the quantum efficiency may be explained by the time difference in connection with changes of the photocathode. However, the main attention may be directed to the of the second order, marked with a black rectangle.

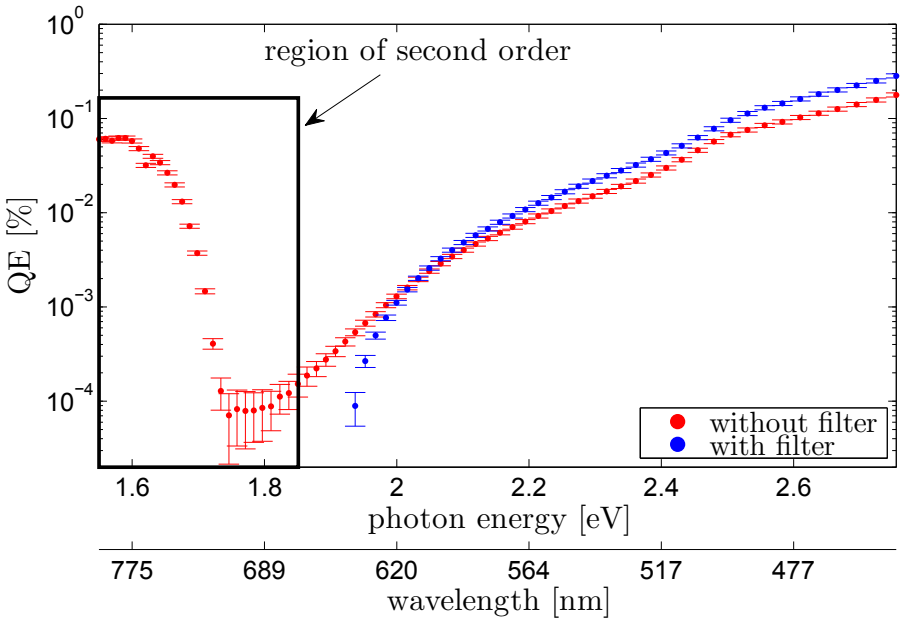

Figure 4.5: Difference in using and not using a filter. The area marked with a □ shows the influence of the second order of the monochromator.

4.5 Spotsize

Thanks to the iris, a stageless change in the spotsize is possible. The smallest possible size of the iris is 0.8 mm [24]. With a magnification $M \sim 0.6$ of the optical path, the smallest possible spot on the cathode should be at about 0.6 mm. To verify this assumption the spot at the cathode was measured with the CCD camera "Prosilica GT 1920" by Allied Vision. Four spotsizes were measured, beginning with the smallest possible one. As diameter, the mean of the FWHM of x and y was calculated. Since the iris is delivered without a scale, only for its lower diameter limit of 0.8 mm, a magnification can be calculated.

With a spotsize of 0.65 mm for the smallest possible iris aperture of 0.8 mm, the experimental magnification of the optical path is given by $M_{exp} \sim 0.8$. In fig. 4.6 there are shown the different spotsizes with its shapes. The length units are given in [pixel]. One pixel has a dimension of $4.54\,\mu m \times 4.54\,\mu m$.

For small spotsizes a flat top profile is formed. For bigger spot sizes remainders of the Xe arc lamp housing are visible, so that the spot is no longer equally illuminated.

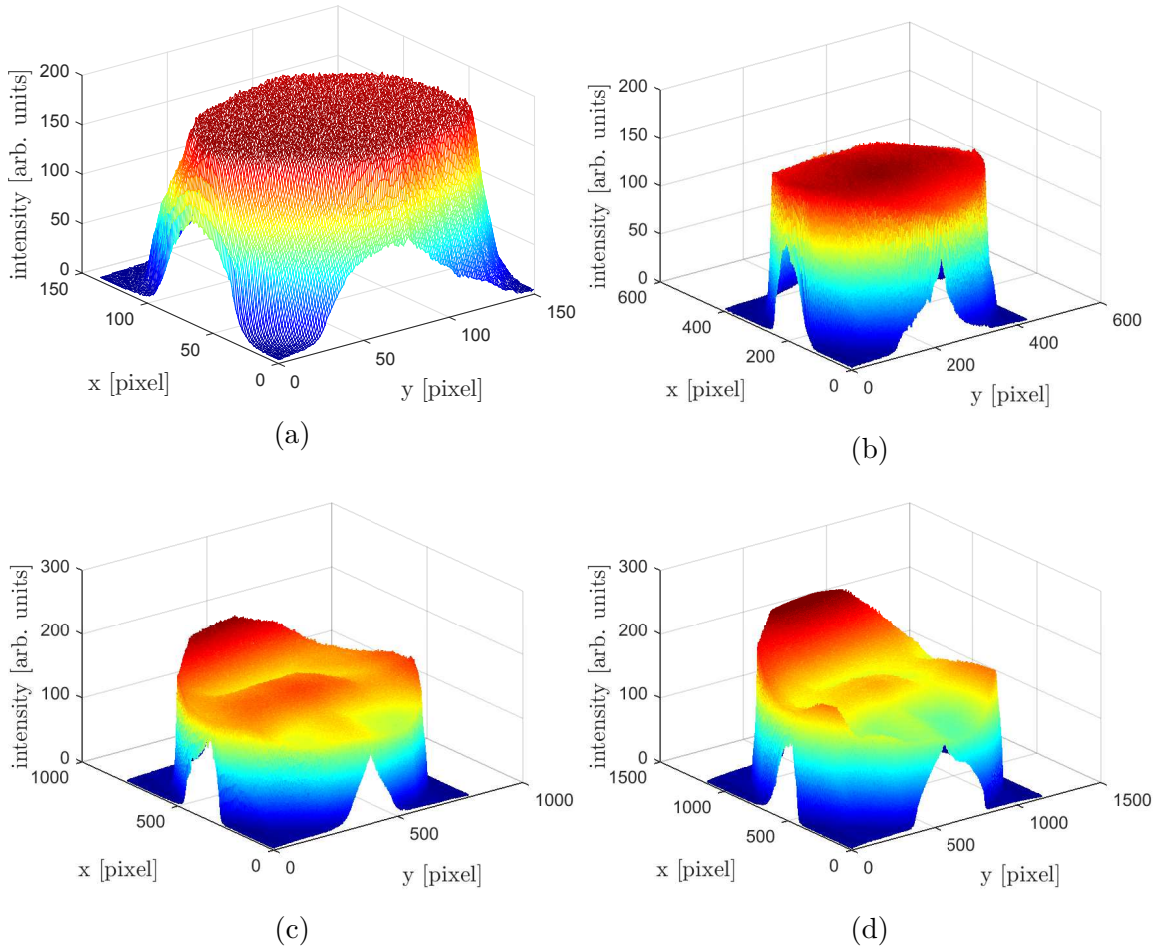

Figure 4.6: Spotsize and spot shape for different aperture diameters, measured at $\lambda = 515\,\text{nm}$ with the CCD camera "Prosilica GT 1920" by Allied Vision. One pixel faces an area of $4.54\,\mu\text{m} \times 4.54\,\mu\text{m}$. The spotsizes were calculated as the FWHM of each maximum:
a) $\varnothing = 0.65\,\text{mm}$, b) $\varnothing = 2.00\,\text{mm}$, c) $\varnothing = 3.50\,\text{mm}$, d) $\varnothing = 5.00\,\text{mm}$.

Besides the shape of the spotsize and its diameter, also the associated power was measured. In fig. 4.7 the power is plotted as a function of the spotsize. The experimental values are fitted with a quadratic function, since the power is a function of the circular area of the spot $P \sim r^2$. The same plot shows the spotsizes in green color.

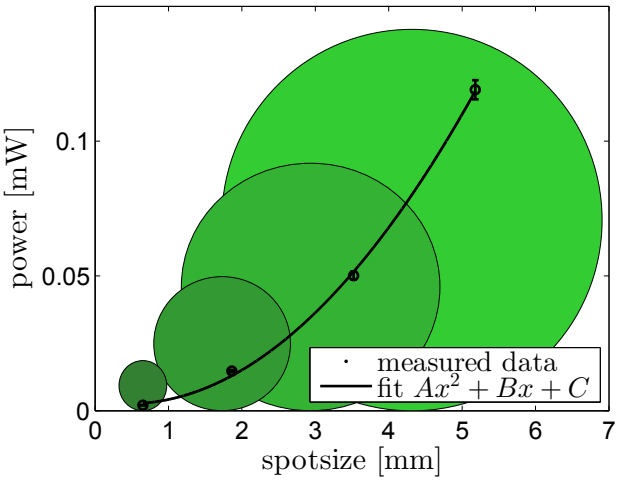

Figure 4.7: Power vs. spotsize at $\lambda = 515\,\text{nm}$. The filled green circles mark the size of the spot.

4.6 Bandwidth

As described in sec. 3.3 the power output, as well as the uncertainty of the wavelength depends on the chosen bandwidth. In fig. 4.8 the power output was measured as a function of the slitwidth. The second axis shows the associated bandwidth expressed as full width half maximum (FWHM). The slitwidth W can be converted to the bandwidth by eq. 3.1. Since there are two rectangular slits (entrance and exit), which can be modified in one dimension, the linear behaviour from eq. 3.1 multiplies to a quadratic behaviour, fitted in fig. 4.8.

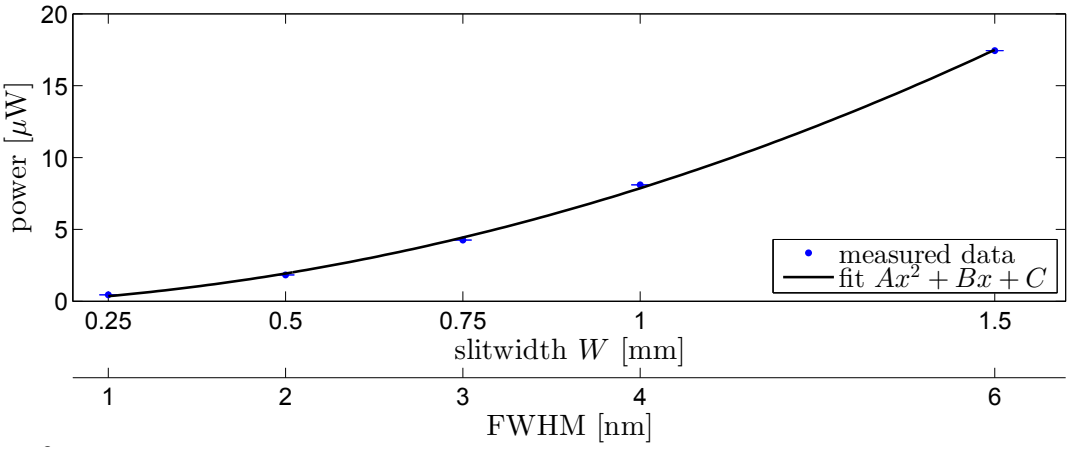

Figure 4.8: Power vs. slitwidth. The slitwidth is correlated to the FWHM of the light and follows a parabola.

As already written in sec. 3.3, a slitwidth of $W = 1\,\text{mm}$ represents a reasonable compromise between the power output and the bandwidth.

4.7 Drift of the Arc Lamp

The Xe arc lamp used in this setup does not provide a constant power output. On the one hand the lamp needs time to reach the desired power output. On the other hand the output is subject to the fluctuation of the Xe arc, producing the light. These parameters were received by measuring the power output for 5 h at 515 nm and a slitwidth of 1 mm, see fig. 4.9. The power output reaches a plateau after $\sim 40\,\text{min}$. Afterwards the fluctuation was calculated as the RMS value, resulting in a relative deviation of $\Delta P/P = 0.08\,\%$.

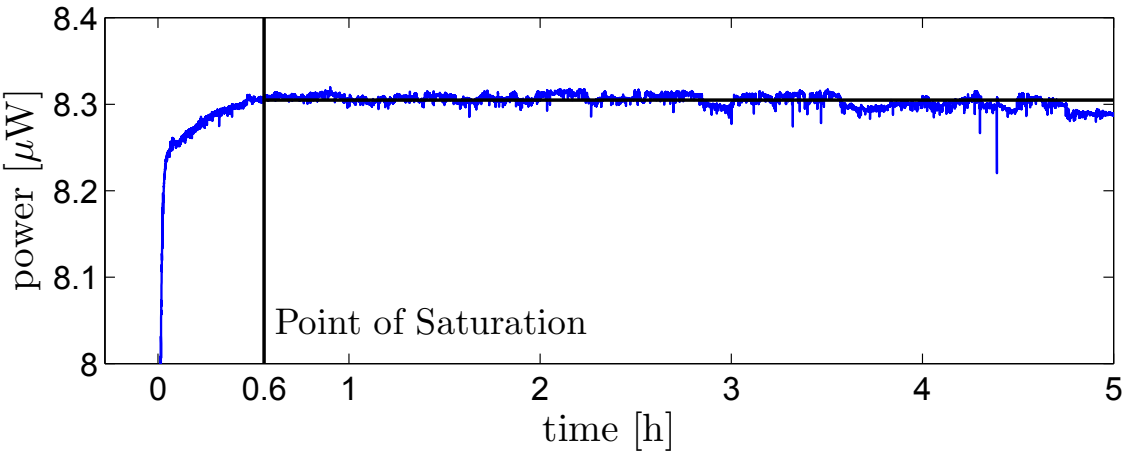

Figure 4.9: Drift of the Xe arc lamp, measured for 5 h at 515 nm.

4.8 Summary of the Commissioning

An experimental setup was successfully commissioned in order to measure the spectral quantum efficiency in a region $\lambda = [400 - 950]$ nm with a maximum power output of $P_{max} = 12\,\mu$W at a bandwidth of 4 nm, fulfilling the requirements of an intense light source, variable in the visible region. The specifications of this setup are shown and recapped in tab. 4.1.

The spectral power can be measured as well as the spectral current. With these values it is possible to calculate the spectral quantum efficiency. The imaged light spot on the cathode is small enough to enable scanning the cathode's surface in order to generate mappings of the quantum efficiency. The monochrome light has a bandwidth ranging small enough to resolve possible spikes in the spectral measurements. Measuring the spectral quantum efficiency with a reproducible uncertainty of 3 %–5 % and an automated setup gives possibility to research the influence of the preparation process on the quantum efficiency and the state of the cathode. This knowledge will help to improve the properties of the cathode concerning the use at GunLab.

parameter	value
wavelength range	400–950 nm (3.4–1.3 eV)
bandwidth ranging	1–5 nm
power output at FWHM= 4 nm	max. 28 μW at $\lambda \approx 470$ nm
spot size on the cathode	0.65–5 mm
stability over time (after 40 min)	0.08 %
magnification of iris aperture	~ 0.6–0.8
rel. uncertainty δQE	3 %–5 %

Table 4.1: Summary of the commissioning parameters.

Further, it is possible to measure the lifetime of the cahode, since this setup provides a stable light source with an uncertainty of $\Delta P/P \approx 0.08$ %.

5 The Preparation of Cs-K-Sb Photocathodes

The preparation of Cs-K-Sb photocathodes takes place in the preparation and analysis system, see fig. 5.1. This system contains a chamber to prepare the cathodes and another chamber to analyse the surface of the cathodes via XPS. Additional, the experimental setup for measuring the spectral quantum efficiency and a transfer system with a vacuum suitcase for the transport of the prepared cathodes to GunLab were integrated. The process of preparation and its validation is described the following sections. All cathodes were prepared by Martin Schmeißer and Julius Kühn. The preparation process of Cs-K-Sb follows the process, given in the handbook of Sommer [25].

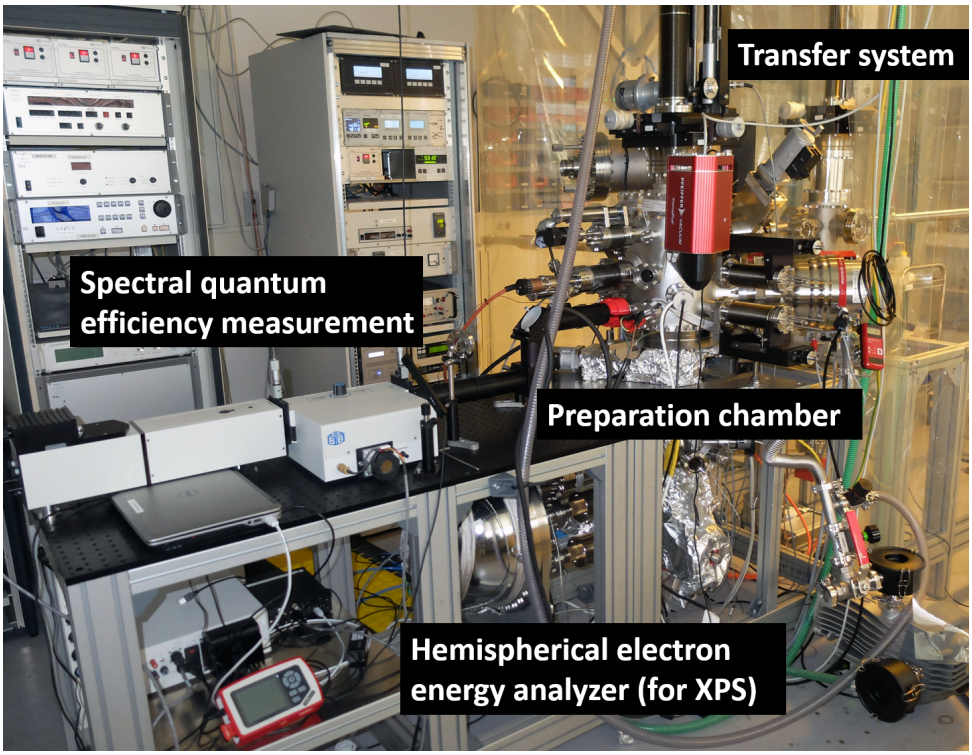

Figure 5.1: View on the cathode lab with the experimental setup for the spectral quantum efficiency (left), the hemispherical electron energy analyzer for XPS (bottom), the preparation chamber (right) and the transfer system (top right).

5.1 Growth Processes

In order to grow a Cs-K-Sb photocathode, different processes are possible. In this work two different growth processes are used. In both cases, a clean, polished Mo plug serves as substrate. The preparation takes place in the preparation chamber, see fig. 5.2.

An effusion cell, loaded with Sb pellets (99.9999%) from Alfa Aesar is used to grow Sb. The preparation with Cs as well as with K occurs by SAES dispensers. The dispensers are located on a different level than the effusion cell, which gives possibility to grow Cs and K either sequentially or by co-deposition. The Sb film has to be grown seperately.

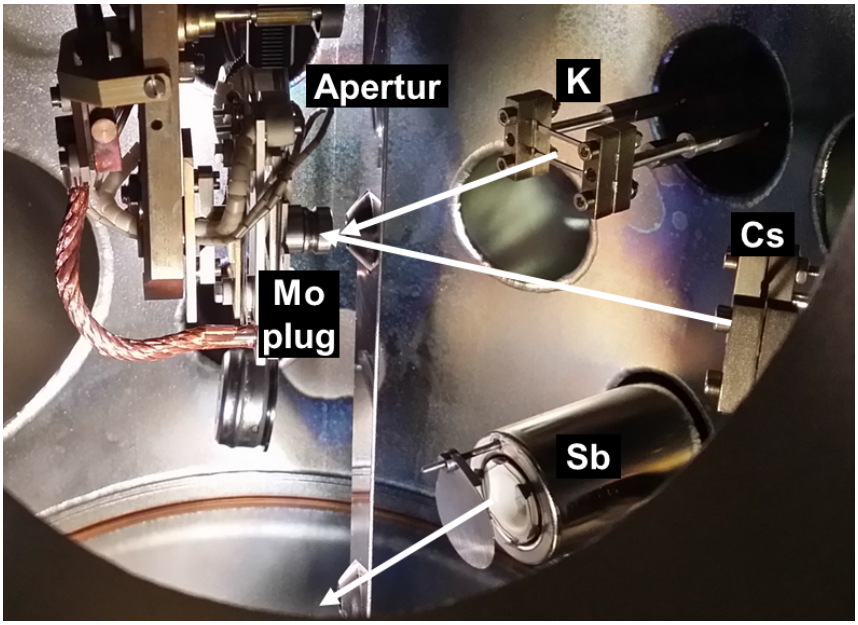

Figure 5.2: Look in the preparation chamber. The Mo-plug can be moved between two levels. On the upper level, K and Cs are grown by SAES dispensers. Sb is grown at the lower level by an effusion cell.

The two growth processes are the sequential growth for the cathode P007 and the co-deposition for the cathode P008, P009, P011 and P013. Both processes are described below with the associated preparation steps and parameters.

5.1.1 Sequential Growth

At the sequential growth Sb, K and Cs are deposited successively. Before the growth process, the pressure of the preparation chamber and the partial pressure of H_2O are recorded. Tab. 5.1 shows the steps for the sequential growth process on the example of cathode P007. The temperature of the Mo plug is set to $T_{sample} = 100\,°C$.

step nr.	step name	parameters
1.	Sb deposition:	rate - 12 Å/min for 8 min 20 s $\hat{=}$ 100 Å = 10 nm
2.	K deposition:	2 SAES dispenser at $I_K = 14\,A$ rate - 1.23 Å/min for 550 min $\hat{=}$ 67.7 nm
3.	Cs deposition:	2 SAES dispenser at $I_{Cs} = 13\,A$ rate - 1.2 Å/min for 100 min $\hat{=}$ 12 nm

Table 5.1: Peparation steps for the sequentially growth by example of photocathode P007. The values for the pressure were $p_{total} \sim 10^{-9}$ mbar and $p_{H_2O} \sim 10^{-11}$ mbar.

5.1.2 Co-Deposition

The co-deposition has some advantages compared to the sequential growth, as there are time savings, better handlings of the growth process and a reduction of the surface roughness [26]. Tab. 5.2 shows the associated steps.

step nr.	step name	parameters
1.	Sb deposition:	rate - 12 Å/min for 8 min 20 s $\hat{=}$ 100 Å = 10 nm
2.	K deposition:	2 SAES dispenser at I_K = 14.2 A for 30 min
3.	K and Cs deposition:	2×2 SAES dispenser at I_K = 14.2 A, I_{Cs} = 14 A for 116 min
4.	Cs deposition:	2 SAES dispenser at I_{Cs} = 14 A for 4 min

Table 5.2: Peparation steps for the co-deposition by example of photocathode P008. The values for the pressure were $p_{total} \sim 10^{-9}$ mbar and $p_{H_2O} \sim 10^{-11}$ mbar.

5.2 Monitoring the Growth Process

In order to monitor the growth process, the photocurrent is measured during each step. To confirm the deposition of Sb, K and Cs onto the Mo plug, X-ray photoelectron spectroscopy (XPS) is performed between every deposition step. Both procedures are described by example.

5.2.1 The Photocurrent

While growing either Sb, K, Cs or K+Cs the photocurrent can be used to monitor the progress of the process. In fig. 5.3 the growth of Cs-K on Sb is shown by example of P008 with a laser of P_{Laser} = 5.40 µW and λ = 400 nm. The peaks resulting from the heater, since it turned on in regular intervals to heat the sample, induced thermal emission of electrons. This emission then was measured by the pA-meter and added up to the photocurrent. The underlying curve represents the actual growth process. It can be seen, that the absolut photocurrent grows slowly in the beginning and changes to a faster increase. Finally a plateau is reached, indicating the end of the growth process. With a fixed deposition rate of Cs, the absolute value of the photocurrent rises in time, while Cs is grown successively. The prior conjunction of K-Sb changes with the amount of Cs, stimulating the photoemission. After a time of ~ 60 min a plateau is reached and the photocurrent does not grow anymore. At this point the growth process is stopped. Afterwards the deposition is verified by XPS, described in the following section.

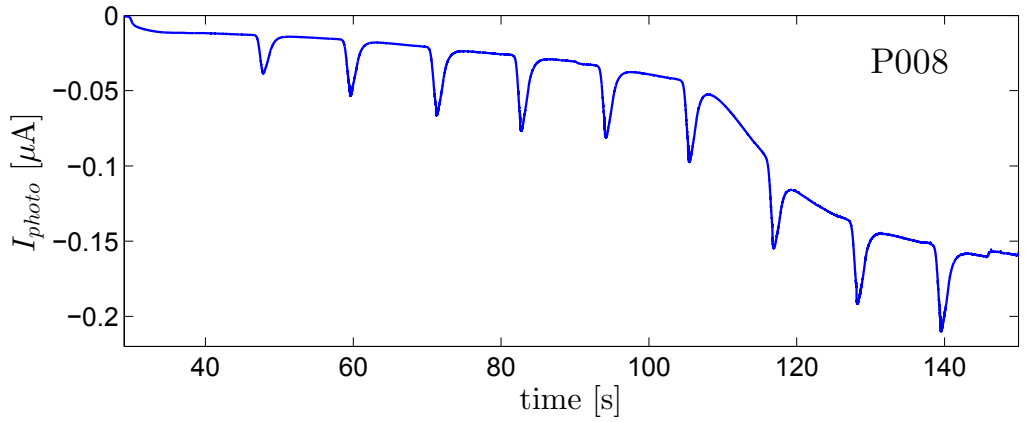

Figure 5.3: Deposition of Cs-K on Sb by the example of P008 with $P = 5.40\,\mu W$ and $\lambda = 400\,nm$. The absolute value of the photocurrent rises in time. The regular peaks are resulting from the sample heater, inducing thermal emission.

5.2.2 X-Ray Photoelectron Spectroscopy

The XPS is based on the photoelectric effect. Surface analysis is accomplished by irradiating a sample with soft Al Kα x-rays at 1489.7 eV and analyzing the energy of the detected electrons. The penetration depth of the photons is limited to an order of 1–10 µm [27].

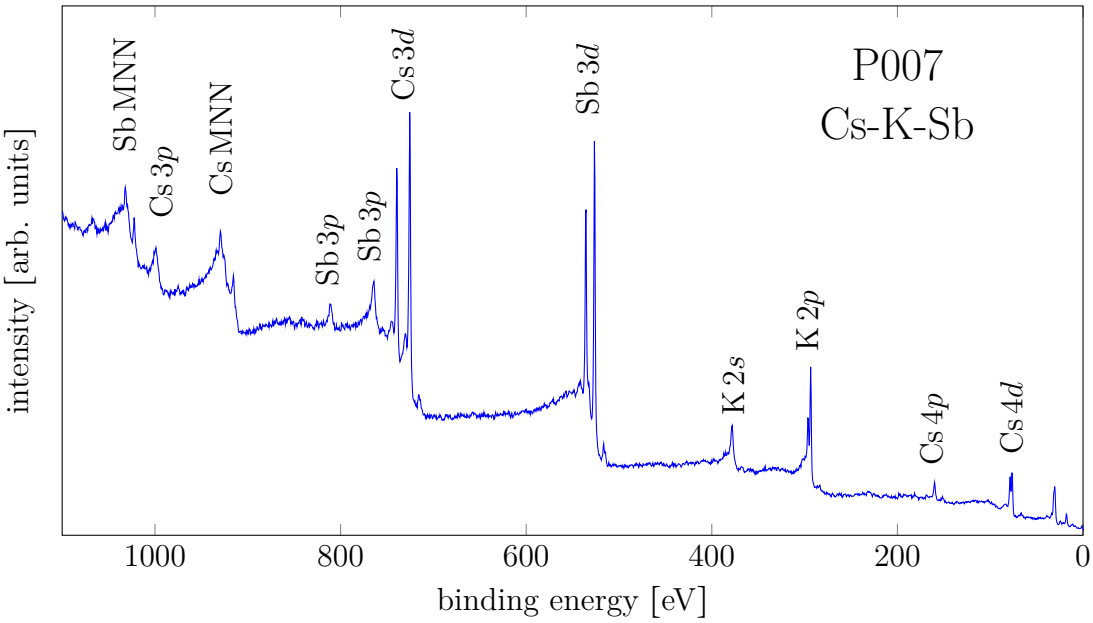

Figure 5.4: X-ray photoelectron spectroscopy survey spectrum of P007, measured with Al Kα (1486.7 eV) radiation.

For the cathode P007 an XP spectrum was recorded right after the growth process, fig. 5.4. Peaks of K, Cs and Sb are visible. Peaks for example of O or Cr would indicate impurities. The most intense peaks may consulted for further analysis. In this case the XPS suffices to validate the existence of K, Cs and Sb on the Mo plug. In order to assign the peaks, the "Handbook of X-ray Photoelectron Spectroscopy" was used [27].

6 Results of the Spectral Quantum Efficiency Measurement

The spectral quantum efficiency was measured for all in all five cathodes at different times. One of these cathodes, to be specific P007, was sequentially grown. The remaining cathodes were grown by co-deposition. This chapter shows the results in the quantum efficiency measurement for all cathodes. Additionally, for P011 and P013, a QE mapping was generated and the lifetime, concerning the QE, was determined.

6.1 Cathode P007: Sequentially Grown

After the growth process, the sample temperature was lowered to $T_{sample} = 90\,°C$. The spectral quantum efficiencies for the steps nr. 2 and 3 in tab. 5.1 are shown in fig. 6.1.

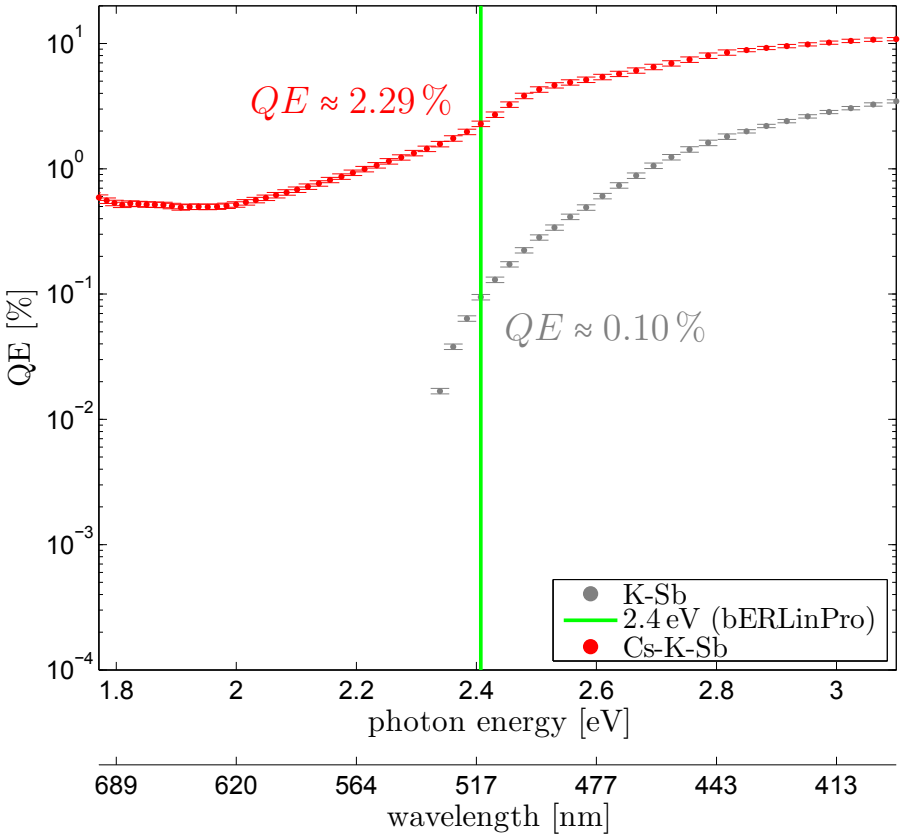

Figure 6.1: Spectral QE of P007 for Sb-K and Cs-K-Sb directly after the growth.

For K-Sb the dark current I_D was measured. After the deposition of Cs, the I_D was not measured again, but rather assumed the same as for K-Sb. This assumption results in a wrong I_D for the first measurement of Cs-K-Sb, reflected in the red plot.

The quantum efficiency in the region of lower photon energy E_γ is higher than for later measurements, where the I_D was recorded for every new measurement. At lower photon energies also the photocurrent should decrease. Instead the dark current remains and contributes to the measured current and the quantum efficiency. This is why the quantum efficiency for Cs-K-Sb in fig. 6.1 does not drop for higher wavelengths. The reason for the difference in the dark current of K-Sb and Cs-K-Sb is, that after the evaporation of Cs onto K-Sb the amount of charge carriers inside the vacuum chamber rises, so that the dark current I_D rises as well.

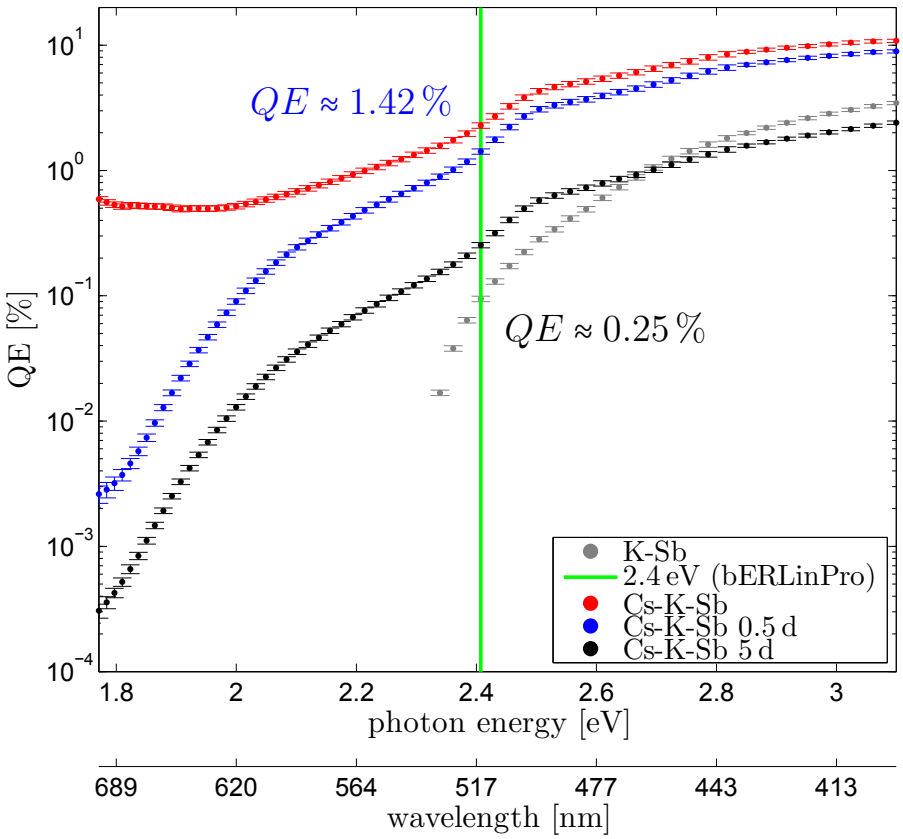

Figure 6.2: The history of the spectral QE of P007.

However, I_D is at least one magnitude lower as the highest measured photocurrent. Hence, in regions of high quantum efficiency the I_D is not significant, so that the measured spectral quantum efficiency in fig. 6.1 in regions $QE > 1\,\%$ is still valid.

6.2 Cathode P008: Grown by Co-Deposition

The cathode P008 is the second cathode measured with the described experimental setup. This cathode was grown by co-deposition.

The temperature of the Mo plug is set again to T_{sample} = 100 °C under the restriction of a loose contact between the sample holder and the sample, so that $T_{plug} \approx 80\,°C$. Table 5.2 shows the steps for the co-deposition on the example of cathode P008. The spectral quantum efficiencies measured for P008 are shown in fig. 6.3 and 6.4. Right after the growth process, the spectral quantum efficiency is lower than after 0.5 days. The reason again is the dark current. For P007 and P008, I_D was measured as a single value and not as an average value over several measurements as is case for the measurement of the spectral power. The spectral quantum efficiency after 0.5 days always remains over $\sim 10^{-3}\,\%$ which indicates, that the value for the dark current does not substract to zero with the measured photocurrent in the region < 690 nm.

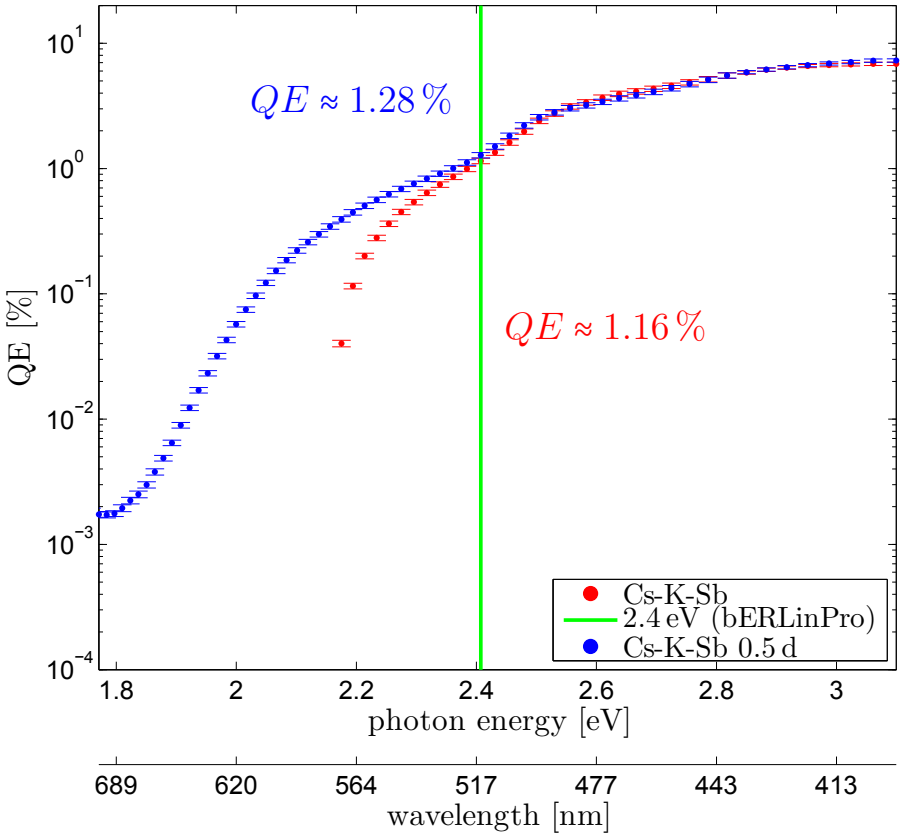

Figure 6.3: Spectral QE of P008 for Cs-K-Sb directly after the growth and after 0.5 days.

To the contrary right after the growth process, the spectral quantum efficiency shows, that the photocurrent falls below the later measured I_D, resulting in a negative value, not displayed in the semilogarithmical plot. This represents an error in the measurement, since the measured photocurrent should be bigger than I_D. In further course, I_D is recorded still seperately, but no longer manually. Its measurement was integrated to the Python routine. A statistical average is formed out of 20 measurements.

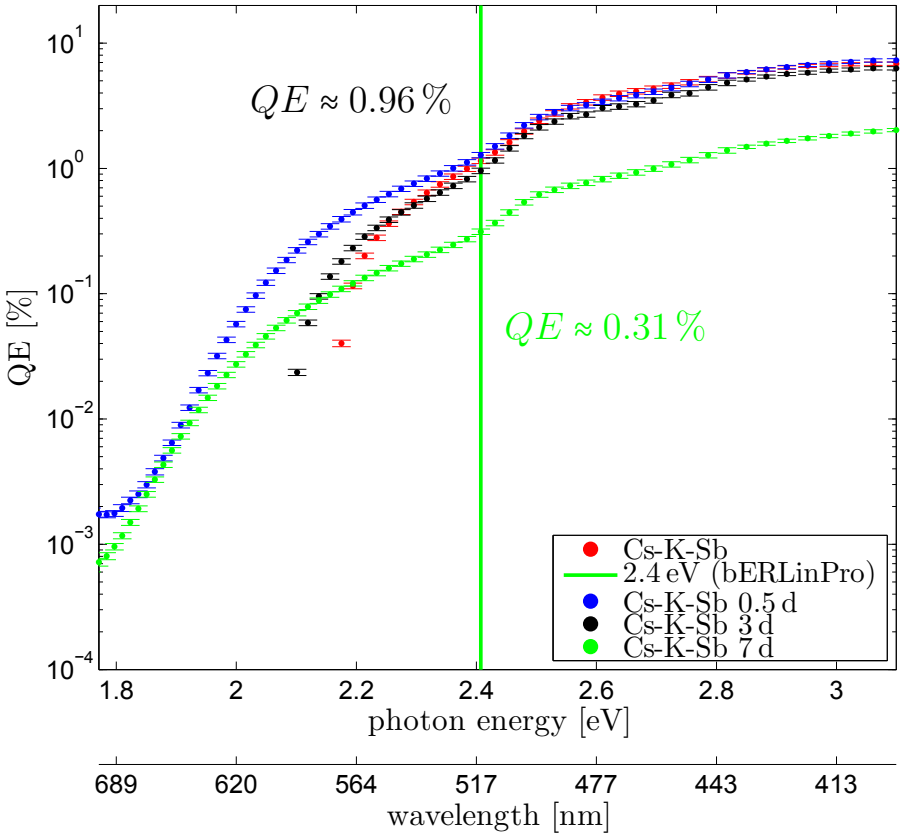

Figure 6.4: The history of the spectral QE of P008.

The quantum efficiencies for P007 and P008 are lower compared to prior photocathodes. The reason for this lies in the loose contact between the sample holder and the sample, resulting in a lower sample temperature than expected. A lower T_{sample} results in a slower reaction between the cathode and the K or the Cs. For further preparations T_{sample} was preventively set to a higher value T_{sample} = 120°C.

6.3 Cathode P009: Grown by Co-Deposition

Like P008, the cathode P009 was grown by co-deposition. Right after the growth procedure the quantum efficiency reached $QE(\lambda = 515\,\mathrm{nm}) = 4.86\,\%$. The transfer system is connected to the preparation chamber, where the cathode is located. Probably owing to a bake out of this transfer system, the quantum efficiency dropped remarkable between day 1 and day 5, see fig. 6.5.

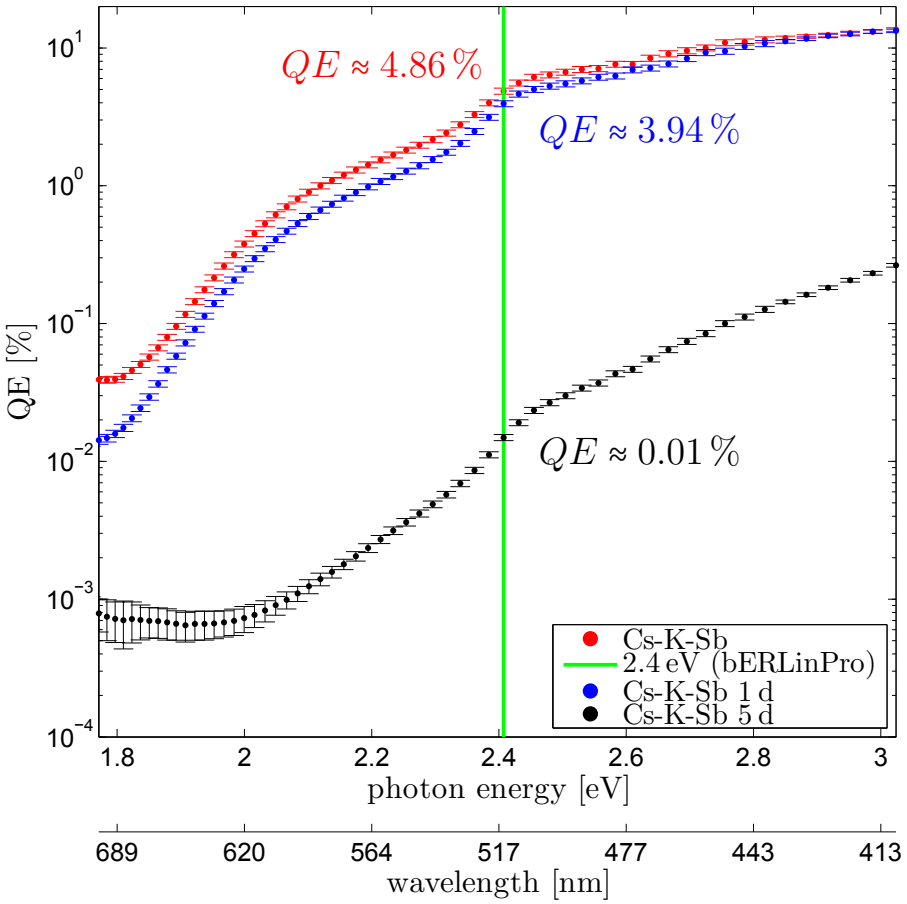

Figure 6.5: Spectral QE of P009 right after the preparation, as well as after 1 and 5 days.

6.4 Cathode P011: Grown by Co-Deposition

Like P008 and P009 the cathode P011 was grown by co-deposition. The initial quantum efficiency is $QE(515\,\text{nm}) = 2.19\,\%$, see fig. 6.6. After 4 days the quantum efficiency dropped to $QE = 0.02\,\%$. In the region $\lambda = [700, 600]\,\text{nm}$ it seems as if the error of the measured quantum efficiency after 4 days growths with smaller photon energy E_γ. This behaviour is due to the logarithmical representation.

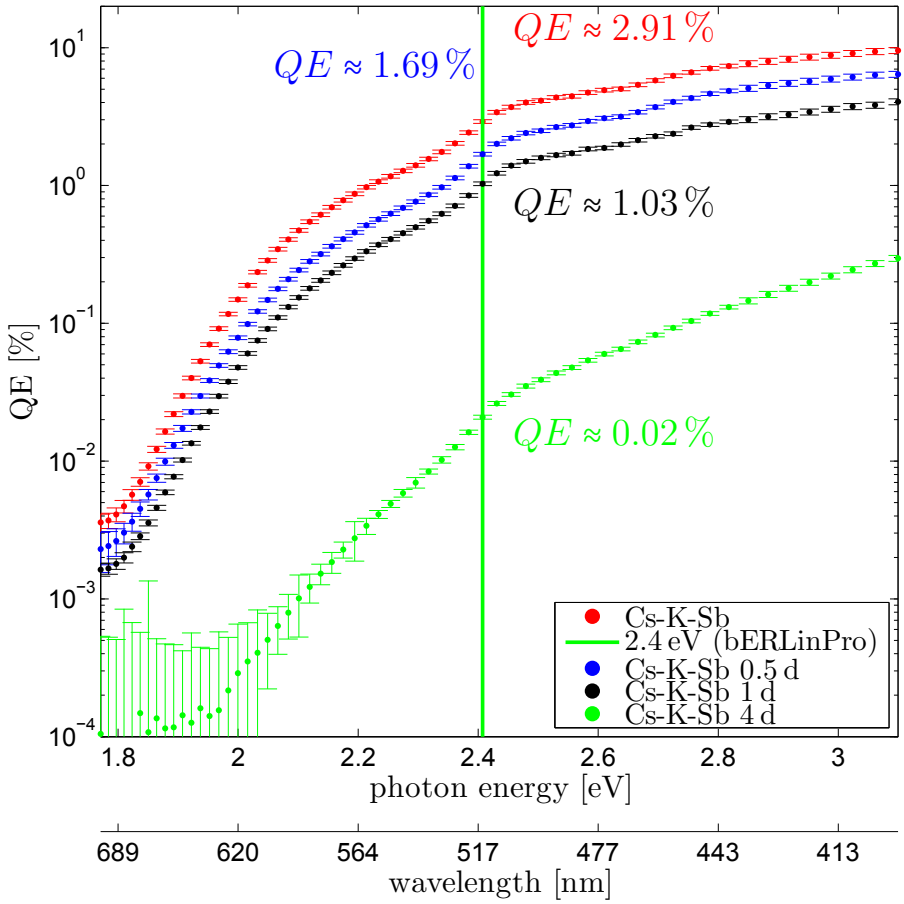

Figure 6.6: The history of the spectral QE of P011.

6.4.1 Mapping of P011

Besides the spectral quantum efficiency, also a mapping of 33 points of the quantum efficiency at $\lambda = 515\,\text{nm}$ on the cathode was generated. The measuring parameters are shown in tab. 6.1. The measuring point were approached by hand, using the manipulator to move the cathode. In fig. 6.7 the mapping is shown with a picture of the completely prepared photocathode as background. The Mo-plug was covered with Sb. Afterwards K and Cs were grown. When preparing the cathodes P007 to P011, the dispensers for K and Cs were not installed perpendicular towards the plug surface and the particle streams had to pass a circular aperture. The result is a Cs-K-Sb region onto the cathode, looking like the Venn diagramm of an intersection.

parameter	value
wavelength λ	515 nm
bandwidth $\Delta\lambda$	4 nm
spotsize $\varnothing$	0.65 mm
duration t_{meas}	12 s
power P	2.01 µW

Table 6.1: Used parameters for the QE-mapping of P011.

The filled rings mark the spotsize onto the cathode as well as the quantum efficiency, which is color-coded. Since the mapping was generated not immediately after the preparation of the cathode, the maximum value for the quantum efficiency decreased to ~ 0.6 %. Also important to mention is the nonuniform distribution of the quantum efficiency even in the Cs-K-Sb region. The highest value is reached right at

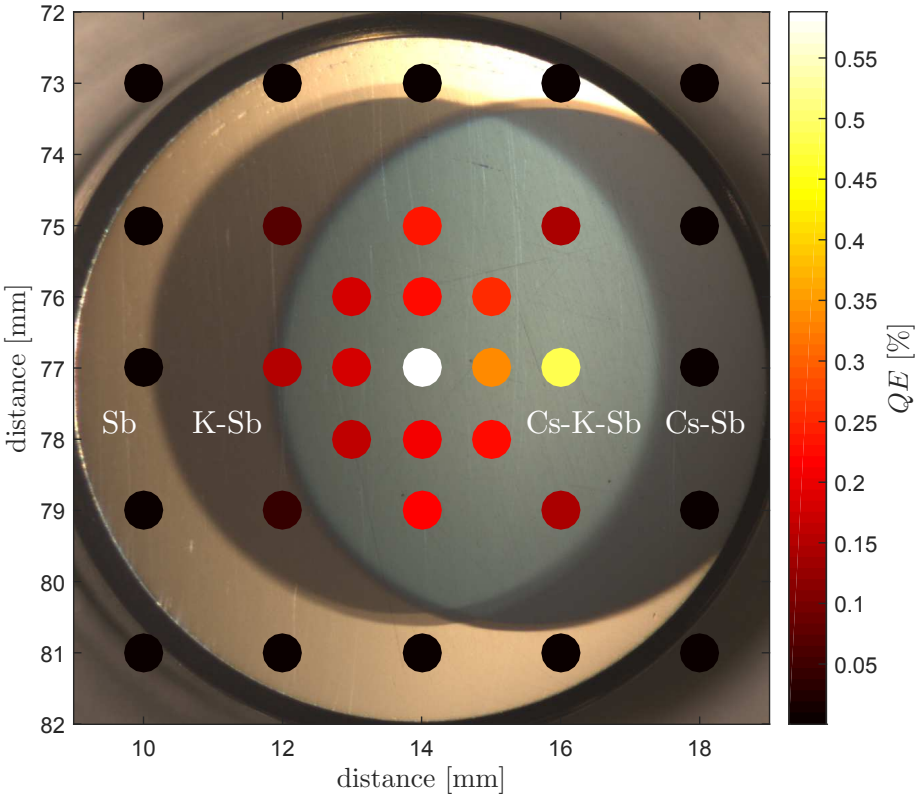

Figure 6.7: QE mapping of P011 at $\lambda = 515\,\text{nm}$.

6.4.2 Lifetime of P011

To determine the mean lifetime of the cathode P011, the photocurrent was measured for nearly 3 days between $QE = [1.03, 0.02]\,\%$. The measuring parameters were the same as in tab. 6.1 except for the longer measuring time. The resulting curve was fitted by an exponential decay, resulting in a mean lifetime of $t_{1/e} = 0.8\,\text{d}$. As for the mapping, it is again important to mention, that the lifetime was not measured directly after the preparation of the cathode, which is why the first value for the quantum efficiency is $QE(t = 0) \approx 0.2\,\%$.

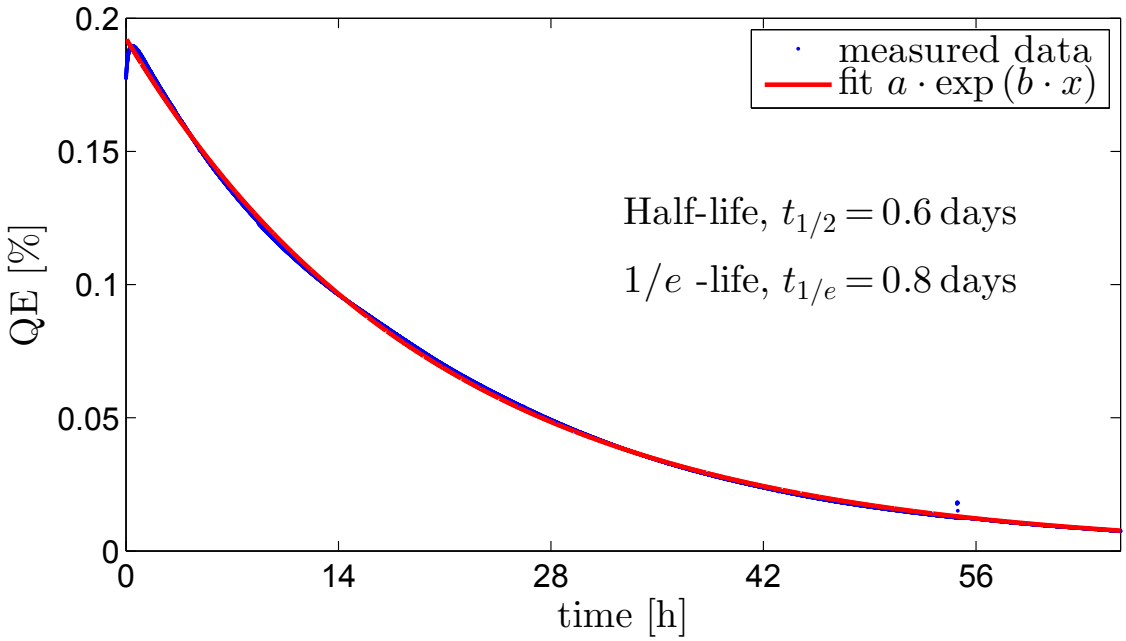

Figure 6.8: Lifetime measurement of P011, measured for ~ 2.5 days at 515 nm. The measurement follows an exponential decay.

Dependance of Thickness of the Sb Film on the Lifetime

There are different results for the lifetime of Cs-K-Sb photocathodes.

Kong et al. [28] measured the mean lifetime as $t_{1/e,K} < 6\,\text{h}$ at $\lambda = 527\,\text{nm}$, which is significant smaller. A higher lifetime was estimated by Dunham et al. [6] with $t_{1/e,D} = 30\,\text{h}$. In contrast Seimiya et al. [29] measured a mean lifetime of $t_{1/e,S} = (5300 \pm 80)\,\text{h}$ at $\lambda = 532\,\text{nm}$ using SUS304 as substrate, which corresponds to a lifetime of about 7 months.

Anyway it is necessary to extend the lifetime of the cathode to improve its application inside the SRF gun. Increasing the thicknes of the Sb film may help to increase the cathodes lifetime. This assumption is supported by the results of Mamun et al. [30], who measured the lifetime of Cs-K-Sb cathodes on Ga-As as substrate, depending on the Sb thickness. The result of this study is, that the lifetime growths with growing Sb film, see fig. 6.9.

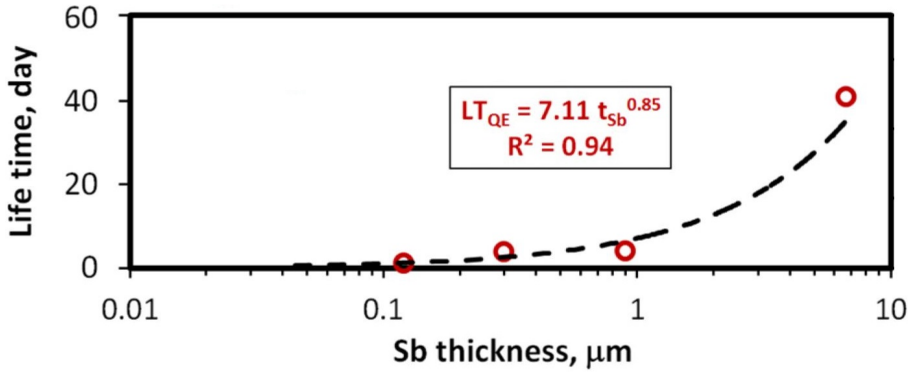

Figure 6.9: $1/e$ lifetime as a function of Sb thicknes for Cs-K-Sb photocathodes deposited on a Ga-As substrate [30].

Dependance of the Vacuum on the Lifetime

Besides the aforementioned thickness of the Sb film, also the vacuum is an important influence on the cathodes lifetime. Looking at the XPS data of all cathodes, it can be seen, that the oxygene peak slowly grows in time, indicating an oxidation process. Therefore, not only the vacuum itself has to be as good as possible, also the mixture of the residual gases is important. An accurate bake-out of the preparation chamber and the outgassing of all filaments and dispensers is important to reduce for example the amount of H_2O. Also the adsorption of CO may influence the cathodes lifetime. But for now, the partial pressure of H_2O is the highest in the residual gases and therefore causing a higher effect. The process of aging itself will be tested in further experiments.

6.5 Cathode P013: Grown by Co-Deposition

The cathode P013 is the last cathode measured for this study. The process of preparation was slightly different from the other cathodes grown by co-deposition. The difference to the preparation of the cathodes P008, P009 and P011 is the temperature. Instead of $T_{sample} \approx 100\,°C$, the cathode was heated up to $T_{sample} = 150\,°C$ before the growth process. The pressure during the process was about $p_{tot} \sim 10^{-9}$, $p_{H_2O} \approx 6 \times 10^{-9}$. During the process the temperature was lowered to 120 °C for further two hours, see tab. 6.2. At this point the photocurrent raised up to $QE(\lambda = 515\,nm) \approx 7\,\%$, indicating the crystallization of Cs-K-Sb to one defined phase.

step nr.	deposition of	parameters	temperature [°C]
1.	Sb	rate - 12 Å/min for 25 min $\hat{=}$ 30 nm	150°C
2.	K+Cs	2 SAES dispenser at $I_K = 13\,A$ and $I_{Cs} = 12\,A$ for 4 h	150°C
3.	K+Cs	2 SAES dispenser at $I_K = 13\,A$ and $I_{Cs} = 12\,A$ for for 2 h	120°C

Table 6.2: Peparation steps for the co-deposition by example of photocathode P008.

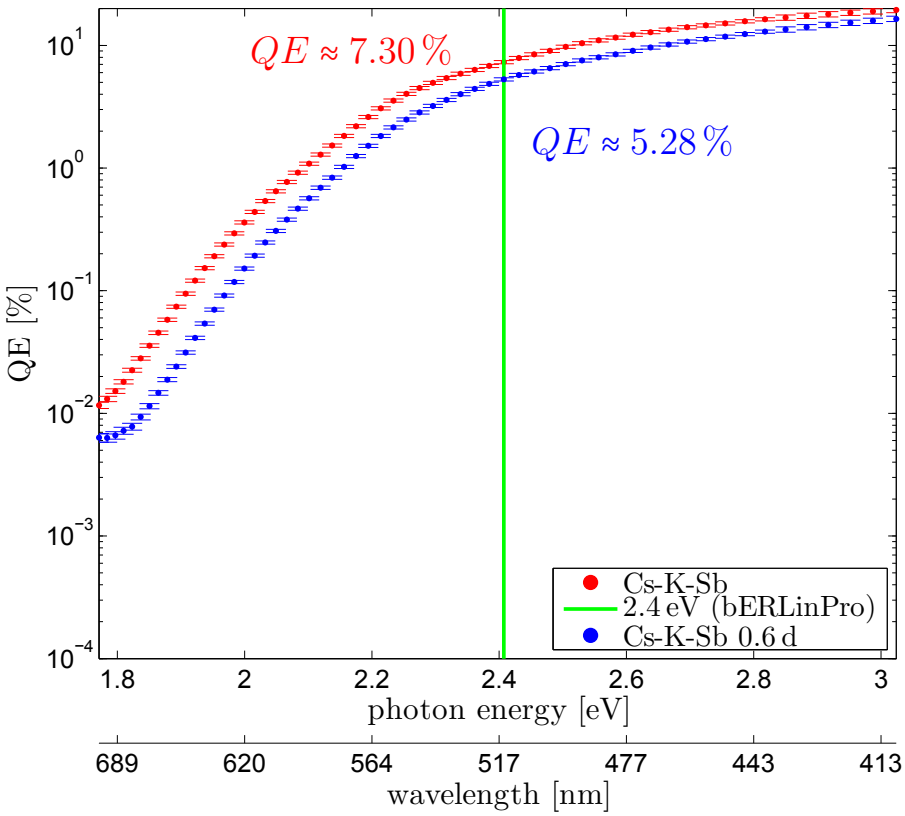

Figure 6.10: Spectral QE of P013 right after the preparation and after 0.6 days.

This assumption is supported by the spectral quantum efficiency, see fig 6.10. The course of the curve is smooth, which differs from the before prepared cathodes. This smoothness as well indicates the crystallization of Cs-K-Sb to just one phase.

6.5.1 Measurement Chronology for P013

Since the cathode P013 showed so far the highest values in the spectral quantum efficiency, many different measurements were performed. The following sections contain different lifetime measurements, a mapping of the quantum efficiency at $\lambda = 515\,\text{nm}$ and the behaviour of the spectral quantum efficiency under cryogenic temperatures. A short list shows the chronology of these measurements:

1. a lifetime measurement of the cathode at the beginning of the cooldown
2. the photocurrent at $\lambda = 515\,\text{nm}$ during the cooldown
3. the spectral QE before, after and during the cooldown
4. as well as the spectral QE after the warm-up
5. the photocurrent during the warm-up
6. a mapping of the QE at $\lambda = 515\,\text{nm}$
7. a long term measurement of the lifetime

All these measurements are shown and explained below.

6.5.2 Lifetime of P013

The lifetime for P013 was measured for about eight hours at $\lambda = 515\,\text{nm}$ with $P_{light} = 5\,\mu\text{W}$, see fig 6.17. For the first 3 hours, the QE saturates to $\sim 5.18\,\%$. This behaviour is comparable to the lifetime measurement of cathode P011, see fig. 6.8.

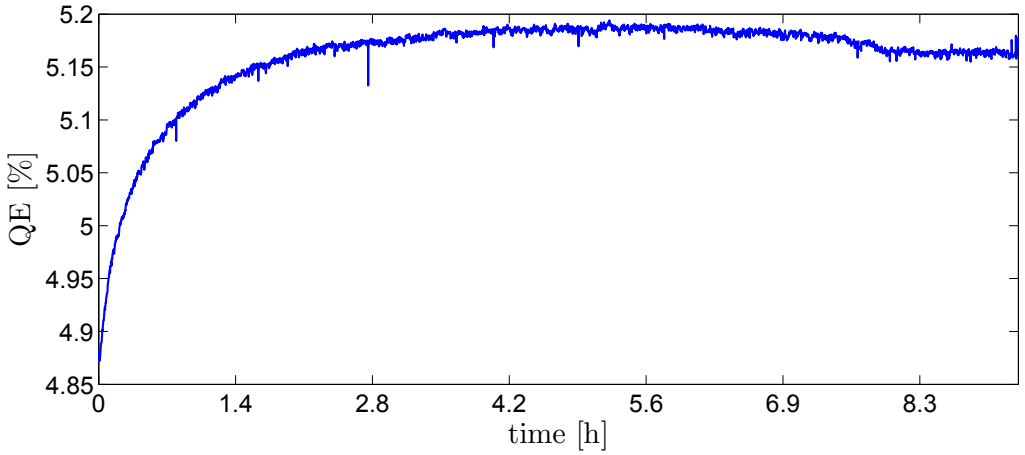

Figure 6.11: Lifetime of P013 measured for about eight hours at $\lambda = 515\,\text{nm}$ with $P_{light} = 5\,\mu\text{W}$. After an initially saturation, the quantum efficiency just slighty decreases.

Afterwards the quantum efficiency stays nearly constant at $QE \approx 5.18\,\%$. A decrease is visible for the last two hours. Since the curve has no obvious exponential decay, the mean lifetime was not determined, but crystallisation of Cs-K-Sb seems to stabilize the quantum efficiency in time, so the mean lifetime for P013 exceeds the lifetime of P011.

A reason for the improved lifetime might be the thicker Sb film of $d_{Sb} = 30\,\text{nm}$. As comparison, the thickness of Sb of the cathodes P008, P009 and P011 was at $d_{Sb} = 10\,\text{nm}$

6.5.3 The Behaviour of the QE at Cold Temperatures

Since the Cs-K-Sb cathode will be installed inside the superconducting RF gun, it is important to know the behaviour of the quantum efficiency when the temperature reaches cold temperatures. Therefore the preparation chamber was uprgaded with a cooling system, using liquid nitrogen to cool the cathode down to temperatures of $T_{sample} \approx -120°C$. During the cooldown, the photocurrent at $\lambda = 515\,\text{nm}$ was recorded, see fig. 6.12. A slight increase of the absolute photocurrent is visible in a range of $\Delta I_{photo} \approx 3\,\text{nA}$, resulting in a change of the quantum efficiency of $\Delta QE \approx +0.1\,\%$. Afterwards the quantum efficiency was measured, see fig. 6.13.

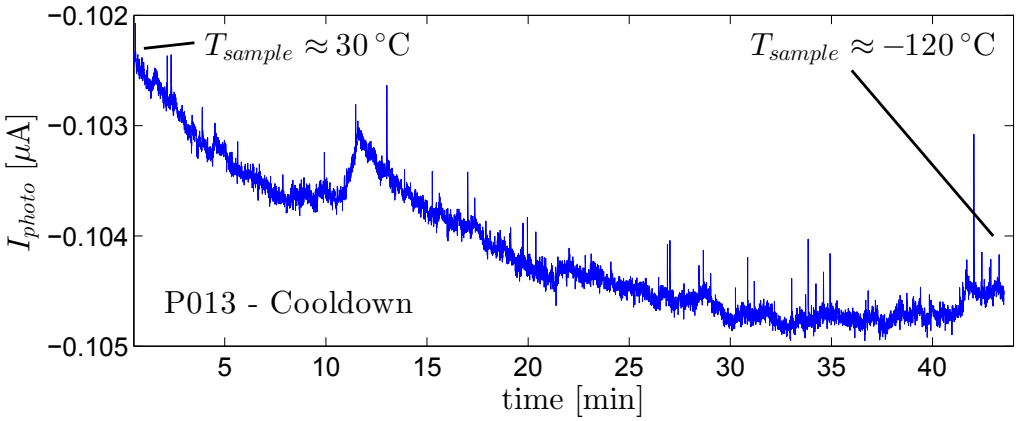

Figure 6.12: Cooldown of P013 for 45 min at $\lambda = 515\,\text{nm}$ with $P_{light} = 5\,\mu\text{W}$. The absolut photocurrent slightly increases with decreasing temperature.

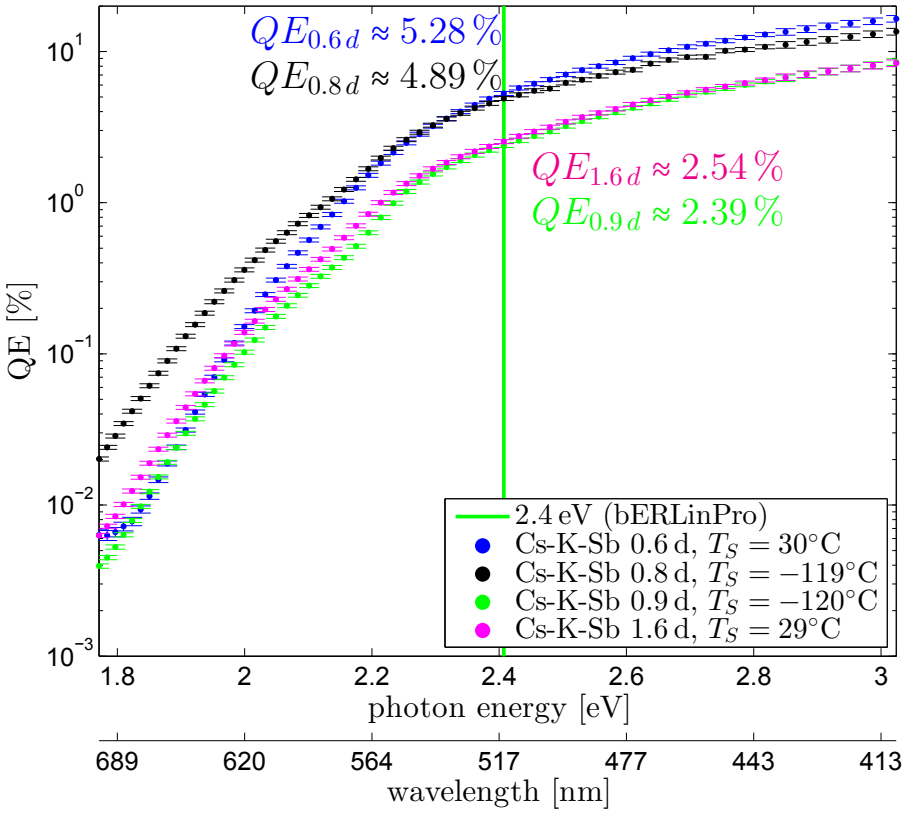

Figure 6.13: Comparison of the spectral QE before and after the cool down to $T_{sample} \approx -120°C$. The QE at $\lambda = 515\,nm$ is not significantly interfered. The decrease in the QE from 0.8 d to 0.9 d is a result of a further measurement in between, that did not took place in the preparation chamber. The cathode had to be moved into a chamber with worse vacuum, wich is why the QE dropped.

Comparing the bare measurement of the photocurrent during the cooldown and the measurement of the spectral QE before and after the cooldown, contrary results are visible, since the first shows an increase of the absolut photocurrent and the second shows a decrease. The reason is the X-ray spectroscopy in between, that took place in the analysis chamber. On the one hand the cathode had to be moved to this chamber, which takes time and on the other hand the pressure in this chamber is worse than in the preparation chamber, inducing a decay of the quantum efficiency at $E_\gamma > 2.3\,eV$. Further, in the region $E_\gamma < 2.3\,eV$ the quantum efficiency increases. To explain this behaviour more measurements might be necessary, since significant statements can not be done. One explanation might be a change in the phase of the cathode. Before the cool down, just one defined phase was visible in fig. 6.10. The increase of the QE at $E_\gamma < 2.3\,eV$ might be due to an additional phase, promoting the photoemission in this region.

During the warm-up between $QE_{0.9d}$ and $QE_{1.6d}$, the spectral quantum efficiency even gained about $\sim 0.1\,\%$. The photocurrent during the warm-up is shown in fig. 6.14. The scale of the photocurrent differs from 6.12 by a factor of 2.

All in all, the process of the cool down and the warm-up did have an influence on the quantum efficiency at $\lambda = 515\,nm$, but the change is not appreciable.

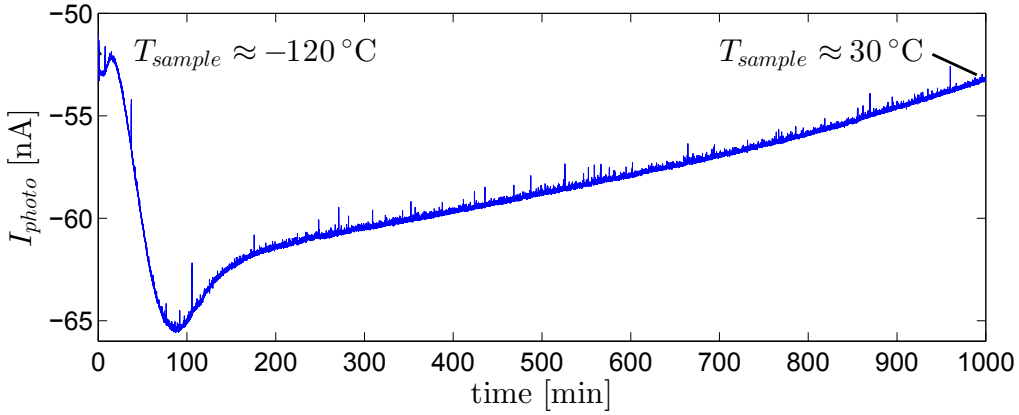

Figure 6.14: Warm-Up of P013 for about 17 h at $\lambda = 515\,\mathrm{nm}$ with $P_{light} = 5\,\mu\mathrm{W}$.

Previous Results on Cold Temperatures

Measurements, concerning the influence of low temperatures were already executed.

Nathan and Mee measured the effect of cooling a Cs-K-Sb cathode on a quartz substrate from 290 K down to 80 K, see fig. 6.15a, whose preparation is described in [31]. Cooling the cathode caused a slight change in the spectral quantum efficiency. For energies lower than 2.2 eV, the quantum efficiency decreases. For energies higher than 2.2 eV, the quantum efficiency increases.

For the region $E_\gamma < 2.2\,\mathrm{eV}$ Xie et al. came to the same results [32]. They cooled down a CsK_2Sb photocathode from room temperature to −107 °C.

In contrast to these results, at KEK also the influence of cryogenic temperature on the quantum efficiency was measured, see fig. 6.15b. This study uses a cathode out of three layers, of which the first is a substrate of $MgAl_2O_4$ with a second layer out of $LiTi_2O_2$. The third layer finally is CsK_2Sb. While the temperature decreases, the quantum efficiency drops from 10 % to ~ 2.5 %. The corresponding photon energy was not mentioned, but a quantum efficiency of 10 % indicates a used energy bigger than 2.4 eV.

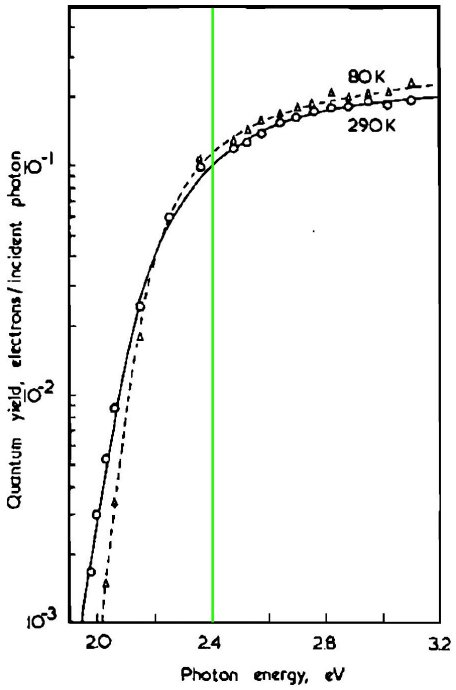

(a)

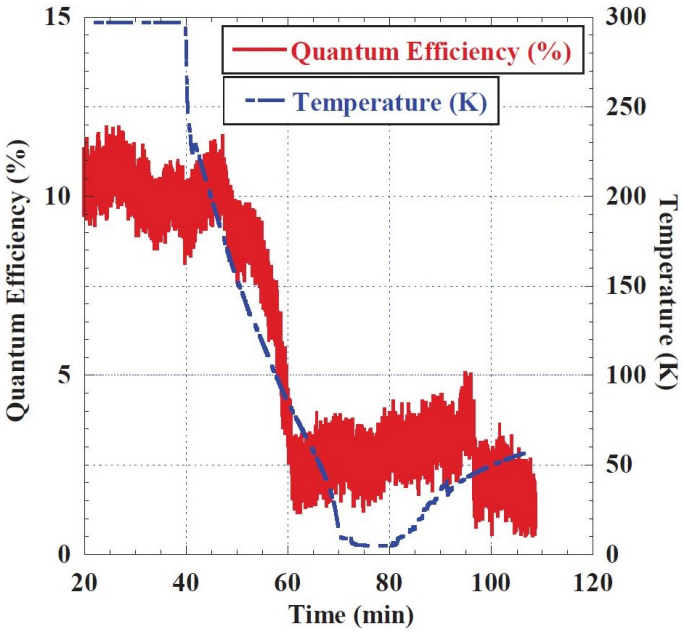

(b)

Figure 6.15: Effect of the temperature on the quantum efficiency:
a) Continous curve, 290 K; dashed curve, 80 K [33]. The photon energy of the laser at bERLinPro is colored in green,
b) KEK SRF-gun cavity [34].

Besides the contrary results of the experiments at KEK, as well as Nathan and Mee at temperatures of $T_{KEK,NM} = 80\,\mathrm{K}$, temperatures at $T_{sample} \approx -120\,^{\circ}\mathrm{C} \mathrel{\hat{=}} 150\,\mathrm{K}$ do not seem to have a signifcant influence on the quantum efficiency at $\lambda = 515\,\mathrm{nm}$.

6.5.4 QE-Mapping of P013

Like for P011, for P013 a mapping of the QE at at $\lambda = 515\,\text{nm}$ was generated. The prepared cathode is shown in fig. 6.16 with the mapping in the foreground. First, the Mo-plug was covered with Sb. Afterwards K and Cs were grown. The cathode was slightly moved during the growth process, which is why the intersection of K and Cs on the Sb film is not as defined as for P011. The measuring parameters are shown in tab. 6.3.

parameter	value
wavelength λ	515 nm
bandwidth $\Delta\lambda$	4 nm
spotsize $\varnothing$	0.65 mm
duration t_{meas}	12 s
power P	2.93 µW

Table 6.3: Used parameters for the QE-mapping of P013.

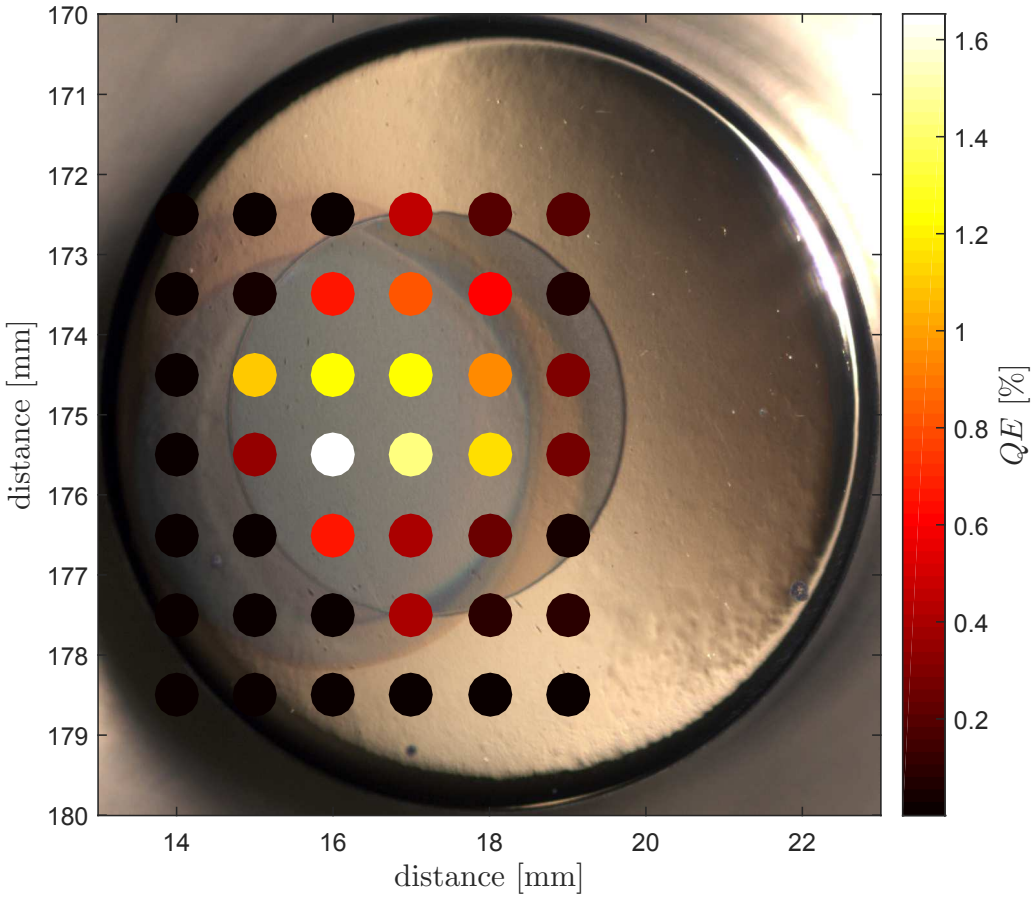

Figure 6.16: QE mapping of P013 at $\lambda = 515\,\text{nm}$. The maximum QE decreased to 1.6 % because of the delay between its measurement and the cathodes preparation.

Again, the spotsize onto the cathode is represented by the colored circles. The quantum efficiency, is color-coded. Although the beginning quantum efficiency of P013 at λ = 515 nm was at about 7 %, the maximum value for this measurement decreased to ~ 1.6 %, since the mapping was generated not immediately after the preparation. Like for P013 the region of highest quantum efficiency is the intersection of Sb, Cs and K, representing the actual Cs-K-Sb photocathode. Leaving this region, the quantum efficiency decreases significantly.

6.5.5 Lifetime after the Cool Down of P013

The lifetime of P013 was again measured after the cool down and the mapping. The same parameters were used as for the lifetime measurement in sec. 6.5.2. Like in sec. 6.4.2, the lifetime was fitted to an exponential decay, resulting in a mean lifetime of $t_{1/e}$ = 0.9 d, see fig. 6.17. This value slightly exceeds the mean lifetime of P011.

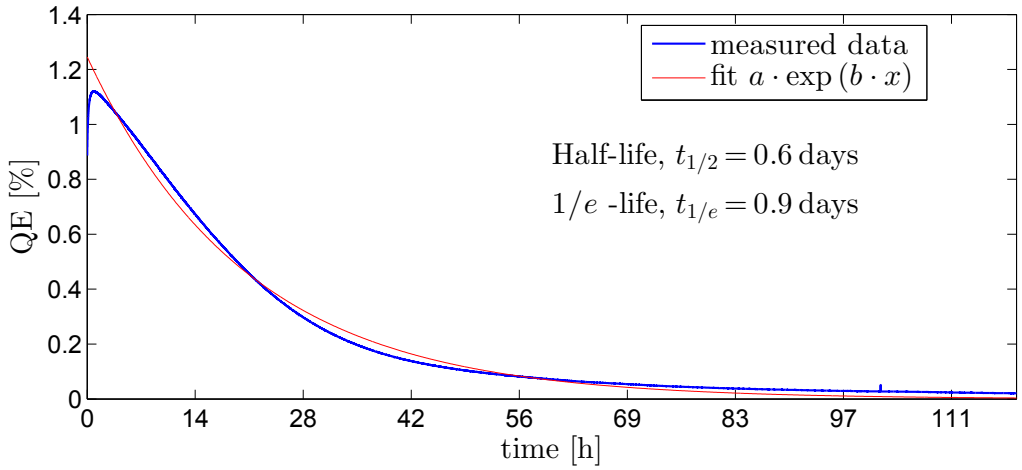

Figure 6.17: Second lifetime measurement of P013 after the cool down experiment for nearly 4 days. Fitting the data to an exponential decay shows a slightly increased lifetime, compared to P011, even after the cool down process.

For all lifetime measurements, an increase in the quantum efficiency is visible from 20 min up to about 3 hours. This increase is an unexpectd process. However, the decay of the quantum efficiency of P011 and P013 fits more or less to the used exponential decay.

7 Interpretation of the Measured Data

In sec. 2.2, the work function ϕ was introduced as the minimum energy needed, to remove an electron from a solid to the vacuum. For semiconductors of one bandgap, the spectral quantum efficiency was derived to eq. 2.11, where the work function is the root. The following sections expand this model to receive two work functions, by assuming two phases inside the solid with two bandgaps and two associated work functions ϕ_1, ϕ_2, which contribute both to the spectral quantum efficiency. Under this assumption a schematic of the spectral quantum efficieny was generated.

7.1 The Determination of Two Different Work Functions

Using eq. 2.11, the spectral quantum efficiency can be simplified. Around the work function ϕ, the parameters l_a and L can be assumed as constant in a narrow region of ν. Then eq. 2.11 can be expanded to a Taylor series of degree one T_1 around ϕ:

$$QE(\nu) = \underbrace{\frac{1}{1+\frac{l_a}{L}}}_{B} \frac{h\nu-\phi}{h\nu} = B(1-\frac{\phi}{x}),\ x = h\nu$$

$$T_1QE(x,\phi) = \underbrace{QE(\phi)}_{0} + \underbrace{QE'(\phi)}_{A}(x-\phi) = A(x-\phi)$$

Thus the spectral quantum efficiency around ϕ can be approximated by the linear function

$$QE(\nu) \approx A(h\nu-\phi). \tag{7.1}$$

Here A and ϕ are constants, in which ϕ can be extracted from a linear fit as the root and A as the slope.

However, the mathematical concept is not based on the sum of two linear functions, since they just would add up to another linear function:

$$\begin{aligned} QE(\nu) &= A_1(h\nu-\phi_1) + A_2(h\nu-\phi_2) \\ &= (A_1+A_2)h\nu - (A_1\phi_1 + A_2\phi_2) \\ &= A(h\nu-\phi),\ A = A_1+A_2,\ \phi = \frac{A_1\phi_1+A_2\phi_2}{A} \end{aligned}$$

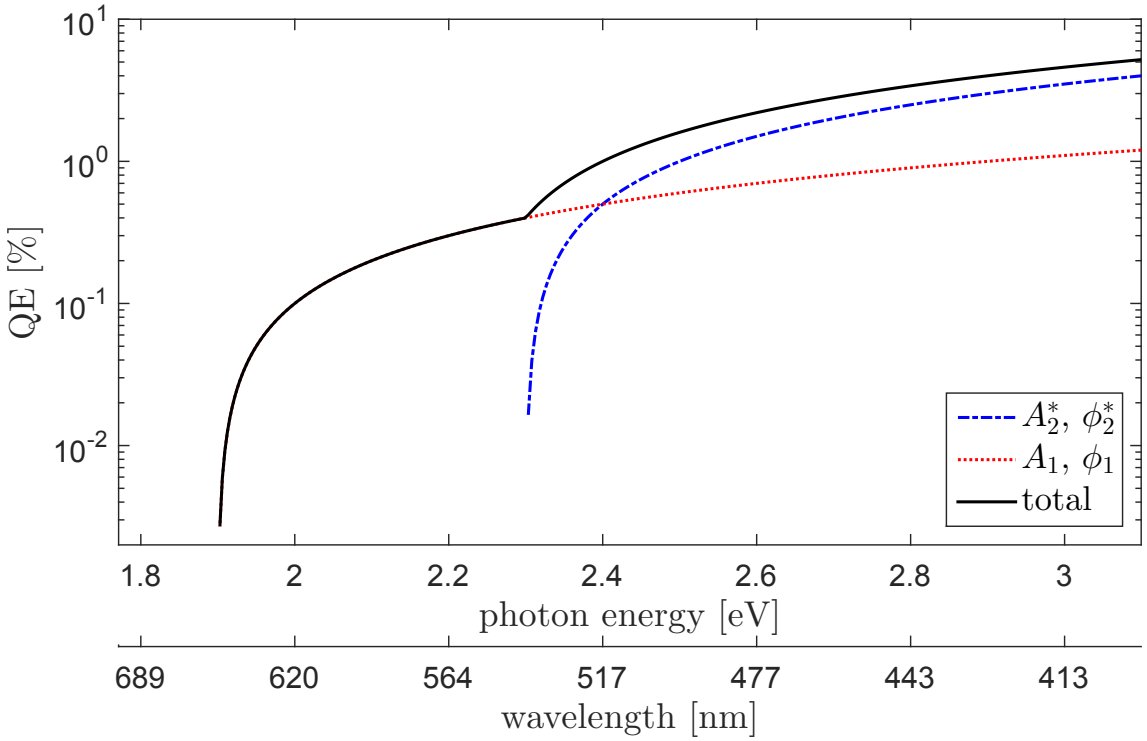

Figure 7.1: Concept plot of two work functions ϕ_1 and ϕ_2^* contributing to the total spectral quantum efficiency.

Rather, this model can be described by two piecewise functions, see fig. 7.1.

$$QE(\nu) = \begin{cases} A_1(h\nu - \phi_1), & \text{for } \phi_1 < h\nu < \phi_2^* \\ A_1(h\nu - \phi_1) + A_2^*(h\nu - \phi_2^*) = A_2(h\nu - \phi_2), & \text{for } \phi_2^* < h\nu \end{cases} \tag{7.2}$$

The work function ϕ_2^* can then be calculated by:

$$\phi_2^* = \frac{\phi_2 \cdot (A_1 + A_2^*) - A_1\phi_1}{A_2 - A_1} \tag{7.3}$$

7.2 Fitting the Spectral Quantum Efficiency

As described in sec. 2.2.2, it is possible to fit eq. 7.1 to the spectral quantum efficiency. The spicer model describes the photoemission process for just one bandgap and therefore also for just one work function. Assuming two different phases inside the cathode, the spicer model can be applied two times, resulting in two different work functions. This procedure was used to fit the previous mentioned photocathodes P007, P008, P009 and P011. A work function ϕ_1 of lower photon energy and a work function ϕ_2 of higher photon energy were determined. In fig. 7.2 the spectral quantum efficiency for P008 was fitted and is shown as an example for the remaining cathodes. Since fig. 7.2 uses a logarithmical y-axis the linear eq. 7.1 appears nonlinear.

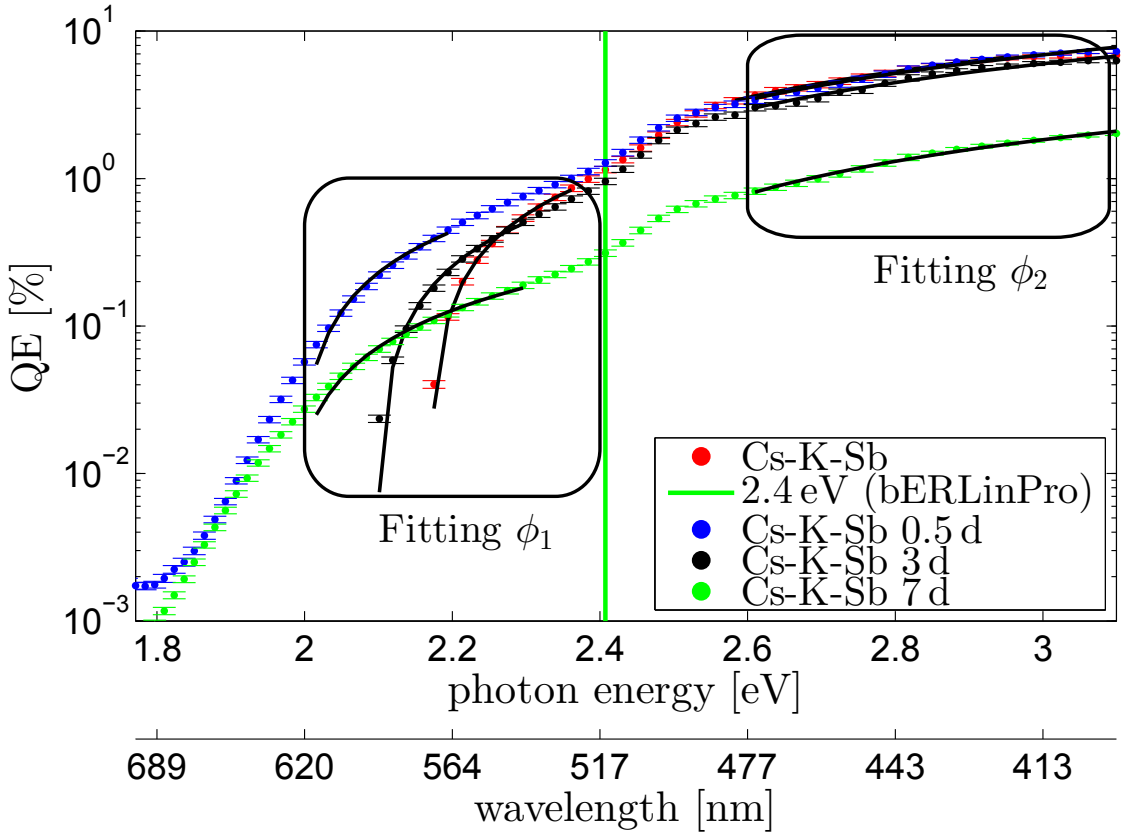

Figure 7.2: Fit of two work functions ϕ_1 and ϕ_2 for P008 as an example.

7.2.1 Comparison of ϕ_1 to Different Models

Since the values of ϕ_1 stay constant in time, the mean value was generated, in order to compare the results for the work function ϕ_1 with literature values. The average is $\overline{\phi_1} = (1.96 \pm 0.02)\,\text{eV}$. The uncertainty was calculated as the standard deviation. Both, the single values for ϕ_1 and the mean $\overline{\phi_1}$ are shown in fig. 7.3.

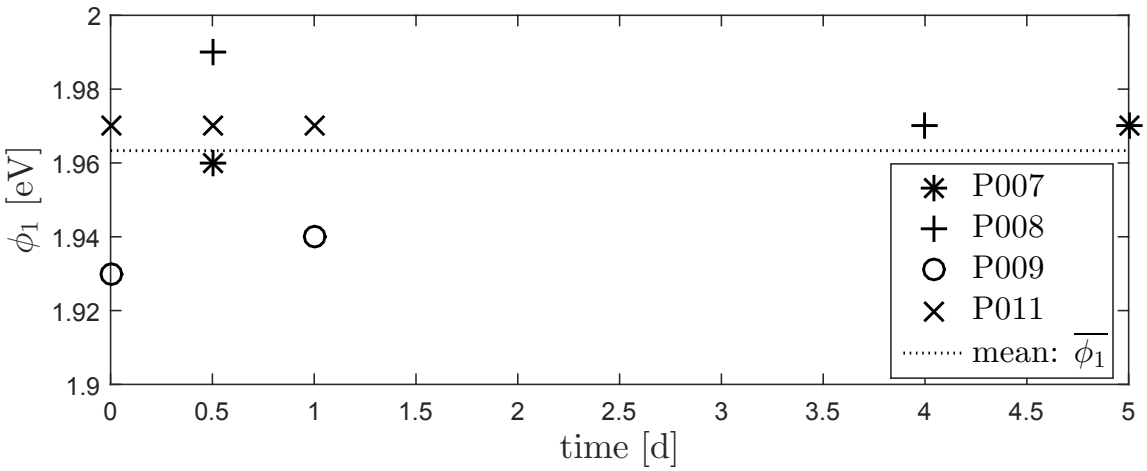

Figure 7.3: All values of ϕ_1 in time for the four measured cathodes. The mean value was generated and is shown by the dotted line.

This value is comparable to those by the papers of Nathan and Mee [33] or Ghosh and Varma [8], see tab. 7.1.

Nathan and Mee used the formula for the spectral quantum efficiency, derived by Spicer in [5] with the optical parameters A and B, treated as constants. Ghosh and Varma used the Kane formula [35], with the constant exponent n, depending on the mode of excitation of the electrons. An error was not mentioned in this study. All presented models are dealing with the work function ϕ as the root.

work	used model for $QE(h\nu)$	results ϕ_i [eV]
this study	$\approx A(h\nu - \phi)$	$\overline{\phi_1} = 1.96 \pm 0.02$
Nathan and Mee	$= A\frac{(h\nu-\phi)^{3/2}}{(h\nu-\phi)^{3/2}+B}$	$\phi_{NM} = 2.10 \pm 0.03$
Ghosh and Varma	$\sim A(h\nu - \phi)^n$	$\phi_{GV} = 1.9$

Table 7.1: Comparison of different studies and the model, used to derive the associated work function ϕ_1 .

The determined work function ϕ_1 lies in between the values of Nathan and Mee, and Ghosh and Varma: $\phi_{GV} < \overline{\phi_1} < \phi_{NM}$. Since the mentioned papers concidered just one work function ϕ_1, only this value could be compared to the associated value from this study. However, ϕ_2^* can be taken into account to have an influence on the quantum efficiency, which will be part of the following subsection.

7.2.2 The Quantum Efficiency as a Function of Time and the Two Work Functions ϕ_1 and ϕ_2^*

Summing up the results for all cathodes, the quantum efficiency can be written as a function of the two different work functions and the time resulting in $QE = QE(\phi_1, \phi_2^*, t)$, see fig. 7.4d. To calculate the work function ϕ_2^* by eq. 7.3, ϕ_2 was used. The projections are shown in 7.4c, 7.4b and 7.4a. Here, the work functions are color-coded with black for ϕ_1 and red for ϕ_2^*. The shapes of the markers are associated to the particular cathode.

Summary of the QE and the fitted work functions ϕ_1 and ϕ_2^* as a function of time

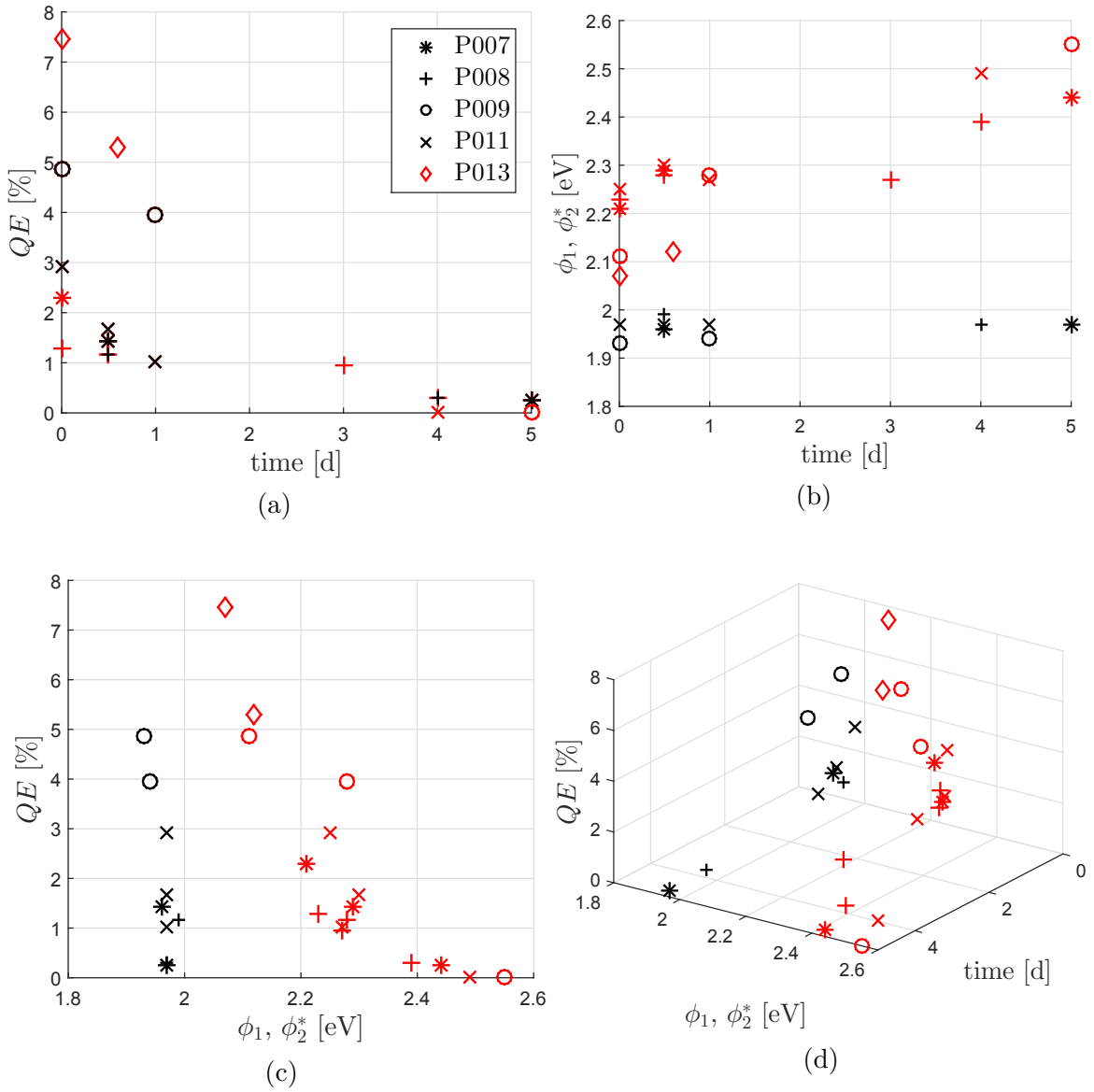

Figure 7.4: The quantum efficiency at $\lambda = 515\,\text{nm}$ as a function of time and the work functions ϕ_1 and ϕ_2^* is shown. Also the work functions are represented as functions of the time:
a) The QE as a function of time drops in time, which conforms to the lifetime measurement for P011 and P013. Starting from different values at $t = 0\,\text{d}$, all quantum efficiencies drop below 1 % after 5 days.
b) The quantum efficiency as a function of the two work functions: $QE = QE(\phi_1, \phi_2^*)$. Like in c), with varying quantum efficiency ϕ_1 nearly stays constant. In contrast the QE drops with ϕ_2^*, indicating, that the quantum efficiency mainly depends on ϕ_2^*.
c) Projection to the plane of work functions $\phi_1 = \phi_1(t)$ and $\phi_2^* = \phi_2^*(t)$, and time. While ϕ_2^* increases in time, ϕ_1 nearly stays constant.
d) The 3D-plot shows $QE = QE(\phi_1, \phi_2^*, t)$.

Looking at the quantum efficiency as a function of the time, a decrease is specifiable. This observation fits with the results of the mean lifetime, see sec. 6.4.2, since the QE seems to follow an exponential decay. After at least five days, the quantum efficiency at $\lambda = 515\,\mathrm{nm}$ is lower than $1\,\%$ for all measured cathodes.

Regarding the time dependency of ϕ_1 and ϕ_2^*, it seems as if ϕ_1 nearly stays constant whereas ϕ_2^* increases. This growth implies, that the photoelectrons need more energy to pass the whole spicer 3 step model. It may be assumed, that Cs volatilizes in time, so that the structure of the associated phase changes and just the bandgap growths, which is associated with an increase of ϕ_2^*. Preparing the cathode so that Cs and preferable also K, remains for longer at the cathode would probably increase its lifetime.

Besides the dependence in time, it is possible to project the quantum efficiency as a function of the work function, so that $QE = QE(\phi_1, \phi_2^*)$. This representation shows, that the quantum efficiency mainly depends on ϕ_2^*. While ϕ_1 stays nearly constant for different quantum efficiencies, the quantum efficiency drops with ϕ_2^*.

Hence, three possible strategies arise to enhance the viability of Cs-K-Sb cathodes for bERLinPro.
Since the quantum efficiency decreases in time, it is necessary to increase its lifetime. The measured mean lifetime of P011 and P013 so far is not convenient for a usage in a SRF gun. Also taking in account, that the cathodes have to be transported from the lab, where they are prepared, to the lab of the gun and inside the gun. For now, an Sb film of 10 nm (30 nm for P013) was used to prepare the cathodes. By growing the Sb film thicker, more Cs may form a chemical compound with Sb. Thus the Cs will rest longer onto the cathode and by that increase the mean lifetime, as measured by Mamun et al. [30].
Another strategy is to decrease the work function ϕ_2^* right after preparing the cathode. In fig. 6.1 the quantum efficiency for P007 rises conspicuously after growing Cs onto K-Sb, which is connected to a decrease in the work function from $\phi_2^*(\text{K-Sb}) = 2.57\,\mathrm{eV}$ to $\phi_2^*(\text{Cs-K-Sb}) = 2.21\,\mathrm{eV}$. By giving the possibility for more Cs to form a compound with the Sb, the work function ϕ_2^* may decrease further. With the same approach of a thicker Sb film, it may be possible to decrease the work function by just growing more Cs onto the cathode.
The third procedure refers to the quantum efficiency itself. By a higher initial quantum efficiency at $\lambda = 515\,\mathrm{nm}$ and a certain lifetime, there is more time until a lower threshold is reached. In the end this method uses the same approach as the aforementioned strategies. In addition, increasing the quantum efficiency will improve its usability inside the SRF gun, since a higher quantum efficiency is correlated to a low laser power. Using high laser power for example will decrease the lifetime of the cathode. Further, it will heat up the cathode, which will affect the superconducting cavity.

8 Summary and Outlook

Cs-K-Sb photocathodes are promising candidates for the generation of high current electron beams, in the visible wavelength region. Thus, in this master thesis an experimental setup was commissioned in order to measure the spectral quantum efficiency of those cathodes in a wavelength region of $[400, 700]\,\mathrm{nm}$.

The setup offers a stable spectral power output, high enough to induce the photoelectric effect on the photocathode. The monochromatic light is focussed on the surface of the cathode and its spotsize can be changed, enabling an integral quantum efficiency measurement as well as a mapping of the quantum efficiency over the cathodes surface. Both, the photocurrent and the spectral power are recorded via an application software. This software was written in Python.

The Cs-K-Sb cathodes were grown by two different methodes. The sequential growth is based on three steps, one for each Cs, K and Sb. Only the cathode P009 was grown this way. The subsequent cathodes were grown by co-deposition, since the simultaneous growth of Cs and K saves time, eases the preparation process and results in smoother photocathodes.

For each cathode several spectral quantum efficiencies were recorded, always right after the preparation process and further after different times. The quantum efficiency at $\lambda = 515\,\mathrm{nm}$ right after the preparation varies in a range of $QE = [1.2, 7.3]\,\%$. The last cathode P013 showed the best quantum efficiency with $7.3\,\%$ because of a slightly changed procedure of the co-deposition process. All previously prepared cathodes showed a behaviour of two crystallizations, while this cathode consists of only one defined crystallization. Further, the lifetime and a mapping of the quantum efficiency was recorded for the cathodes P011 and P013. Both of them showed an exponential decay in the quantum efficiency, indicating a mean lifetime of less than 1 day. The mapping showed a non-uniformly distributed quantum efficiency over the Cs-K-Sb surface, but a maximum in this area was significant.

Further, the behaviour of the spectral quantum efficiency for P013 was measured, when cooled down to $T_{S,1} = -120\,^{\circ}\mathrm{C}$ and afterwards warmed-up to $T_{S,2} = 30\,^{\circ}\mathrm{C}$. During the cool down, the spectral quantum efficiency increased, when going to the infrared region and decreased, when going to the UV region. Right at $\lambda = 515\,\mathrm{nm}$ ($E_\gamma \approx 2.4\,\mathrm{eV}$) the quantum efficiency just changed at about $\Delta QE \approx -0.3\,\%$, which also may be induced by the typical decay of the quantum efficiency in time. The warm-up showed a slight increase of the quantum efficiency of about $\Delta QE \approx +0.2\,\%$. In order to explain these processes, further measurements have to be done. However, at first approximation, the process of cooling down and warming up had no significant effect on the quantum efficiency at $\lambda = 515\,\mathrm{nm}$.

All spectral quantum efficiencies were fitted to the Spicer model in order to extract the work function. Before, this model was simplified by a series expansion of degree one around the work function. Since the cathodes P009 to P011 showed two crystallizations, the model was applied two times in order to receive two different work functions ϕ_1 and ϕ_2^*. Extracting two work functions marks a new sort of treatment of the spectral quantum efficiencies, since all previous studies just assumed one work function ϕ_1. The cathode P013 only showed one crystallization, which is why just one work function was fitted. These values were correlated with the quantum efficiency at $\lambda = 515\,\mathrm{nm}$ and the associated measuring time.

A time dependence of ϕ_1 was not noticeable. In contrast, the quantum efficiency as well as the value for ϕ_2^* showed an opposed behaviour, since the quantum efficiency follows an exponential decay and ϕ_2^* increases in time, indicating a dependence of the QE on this work function. This assumption is covered by plotting the QE as a function of the two work functions. There is just a slight change in ϕ_1, when the QE changes, while ϕ_2^* significantly grows, when the QE drops, which can be inversed. Increasing the work function ϕ_2^* leads to a higher quantum efficiency.

Summing up, the required effort to establish an experimental setup for measuring the spectral quantum efficiency pays back by a deeper insight to parameters of the cathode, like the lifetime, the work function and the quantum efficiency itself. These data will help to optimize the cathode for its use at bERLinPro.

Outlook

An upgrade of the setup to λ = 350 nm would help to optimize the cathodes behaviour in the UV-region. But dealing with UV radiation entails two main challenges. The optical path had to be optimized, since the used lenses and mirrors in the described experimental setup are optimized for a region $\lambda \geq 370$ nm. Going to this wavelength, the power of the light reduces drastically, when arriving on the cathode, since the transmission of the optical path approaches zero. This results in a small signal-to-noise ratio. Also the viewport has to be considered, since it is not transparent in the UV-region. Further, UV radiation brings the problem of toxic ozone under atmospheric air. Therefore, the Xe arc lamp housing would have to be vented with nitrogen.

With the described method of measuring the spectral quantum efficiency, it is possible to determine two different work functions. Another method of determining a samples work function is the Kelvin probe measurement. This technique measures the contact potential difference between two surfaces brought in close proximity, without any electrical contact between them. Since this technique only recognizes a difference in the contact potential, it is necessary to know the work function of the probe used, in order to receive the work function of the sample.

List of Figures

A Contribution to European Workshop on Photocathodes for Particle Accelerator Applications 2016

- Event: European Workshop on Photocathodes for Particle Accelerator Applications 2016 in Daresbury, Great Britain
- Contributors: H. Kirschner, M. A. H. Schmeißer, J. Kühn, G. Klemz, T. Kamps, A. Jankowiak

H. Kirschner, M. A. H. Schmeißer, J. Kühn, G. Klemz, M. Bürger, T. Kamps, A. Jankowiak,
Helmholtz-Zentrum Berlin für Materialien und Energie GmbH, 12489 Berlin, Germany

HZB Helmholtz Zentrum Berlin

Spectral QE-Measurement on a CsK_2Sb Photocathode for bERLinPro

Motivation

The generation of high brightness electron beams for bERLinPro requests reproducible and robust photocathodes with high QE and long operation lifetime. The spectral QE in the visible light spectrum is an important figure of merit. It will help to optimize the process of preparation of the cathode. Furthermore the understanding of the solid state properties of the cathode will be improved.

The Experimental Setup

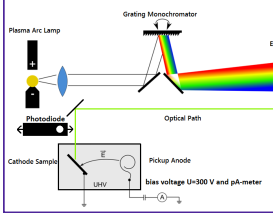

- White light from a Xe arc lamp
- Visible spectrum out of a monochromator
- Optical path from monochromator to cathode
- Measuring the photocurrent versus incident wavelength

The implemented setup allows to change easily between measuring the photocurrent and the spectral flux. Hence, calculating the QE is possible using this equation:

$$QE(\lambda) = \frac{N_e}{N_\gamma} = \frac{I/e}{P_{Light}/E_\gamma} = \frac{I}{P_{Light}} \cdot \frac{1239\,\mathrm{eV\,nm}}{\lambda\,[\mathrm{nm}]}$$

$$QE(E_\gamma) = \frac{N_e(E_\gamma)}{N_\gamma(E_\gamma)} = \frac{I(E_\gamma)}{P_{Light}} \cdot E_\gamma$$

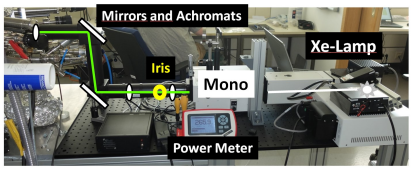

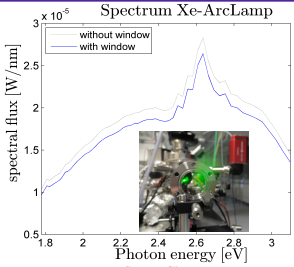

- Spectral flux depends on the wavelength
- Peak at ~470 nm
- depends on the transmission of single components
- e.g. transmission of flange window shown here

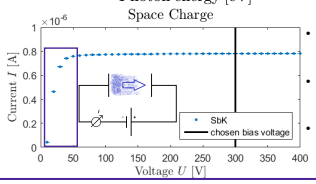

- electrons block the E-field of cathode and anode
- U has to be high enough to yield all electrons
- U_{bias} = 300 V is adequate

First Spectral Response Measurements

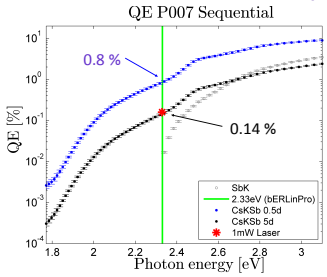

P007 is a sequentially grown photocathode. First K was evaporated onto Sb, then Cs. After each step the spectral QE was measured. To get information of the cathode's lifetime, measurements up to 5 days have been done. The setup delivers comparable results to a laser at 2.33 eV.

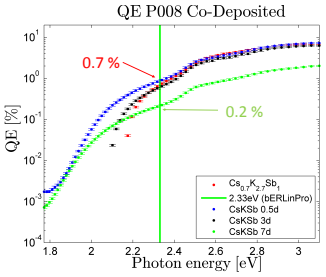

P008 is a co-deposited photocathode. K and Cs were evaporated simultaneously onto Sb. Several measurements were done to again get information of the cathode's lifetime as well as the spectral QE right after the codeposition.

Summary

- An experimental setup was developed and attached to the Photocathode Prep. System
- Spectral QE of two Cs-K-Sb photocathodes was measured
- Results are comparable to a laser with fixed wavelength of 532nm

Outlook

- Determination of the Xe arc lamp's spectral flux stability over time
- Monitoring the photocathode's life time
- Fit-model (Spicer) to calculate the work function
- Mount Low pass filter to remove second order of the monochromator grating
- Change the software from MATLAB to python

Hans Kirschner| hans.kirscher@helmholtz-berlin.de | European Workshop on Photocathodes for Particle Accelerator 2016, Daresbary, UK.

www.helmholtz-berlin.de

B Python Program to Measure the Spectral Quantum Efficiency

The main program to measure the spectral quantum efficiency consists out of two subsidiary programs, one to measure the spectral power and the other to measure the spectral current. It is necessary to record both for every spectral quantum efficiency measurement, in order to consider possible changes e.g. of the spectral power. Both parts are listed below.

B.1 Measuring the Spectral Power

Opening the Power Meter: `openPM.py`

Before the spectral power can be measured, it is necessary to open the power meter as an object inside python:

```
1  # -*- coding: utf-8 -*-
2  """
3  Created on Tue Aug  2 12:10:41 2016
4
5  @author: pcalab
6  """
7  def openPM(visa):
8      ## open Power Meter via right USB port
9      rm=visa.ResourceManager()
10     print(rm)
11     print(rm.list_resources())
12     PM=rm.open_resource(\
13     'USB0::0x1313::0x8078::P0013049::0::INSTR')
14     print(PM)
15     ## ask for ID number
16     IDN=PM.query('SYST:SENS:IDN?')
17     print(IDN)
18
19     ## set possible wavelength range,
20     ## depending on the diode
21     maxBer=1100
22     ## S130VC
23     if IDN[4]=='V':
24         minBer=200
25     ## S130C
26     elif IDN[4]=='C':
27         minBer=400
28
29     return PM, minBer, maxBer
```

Measuring the Spectral Power: `Leistung.py`

After the power meter was opened, the monochromator motor is triggered in a certain wavelength region, devided into a certain stepsize in order to measure the spectral power:

```
# -*- coding: utf-8 -*-
"""
Created on Thu Aug  4 11:11:49 2016

@author: pcalab
"""
## import modules
import PM_Meas
import time
import matplotlib.pyplot as plt

def Leistung(PM,WL,Bereich1,Bereich2,DefBer,\
                 WrtBer,Std,Zeit,Steps,f,Mono):
    ## moving motor to dedicated range and steps
    for i in range(len(DefBer)):
        print(Bereich1+i*Steps)
        Distance2=((Bereich1-WL)+i*Steps)*f
        move2="X" +str(Distance2) +"g"
        Mono.write(move2)
        time.sleep(3)
        ## power measurement
        WrtBer[i],Std[i],Zeit[i]=\
        PM_Meas.PM_Meas(Bereich1+i*Steps,PM);
        time.sleep(1)

        ## ploting the measured data
        # fig=plt.figure()
        plt.scatter(DefBer[0:i+1],WrtBer[0:i+1])
        plt.axis([Bereich1, Bereich2,min(WrtBer[0:i+1]),\
                  max(WrtBer[0:i+1])])
        plt.show()

    ## save data and figures and return them
    P_cont=DefBer,WrtBer,Std,Zeit
    fig=plt.figure()
    plt.scatter(DefBer[0:i+1],WrtBer[0:i+1])
    plt.axis([Bereich1, Bereich2,min(WrtBer[0:i+1]),\
                max(WrtBer[0:i+1])])
    return P_cont,Mono,fig
```

A Single Power Measurement: `PM_Meas.py`

The power is measured for each wavelength step:

```
# -*- coding: utf-8 -*-
"""
Created on Thu May 12 09:18:31 2016

@author: pcalab
"""
## import modules
import time
import numpy as np
def PM_Meas(WL,PM):
    ## record time
    Zeit=time.strftime("%Y%m%d%H%M%S")
    number=100  # number of measrements

    ## do 100 measurements
    PM.write('Timeout 10')
    PM.write('EOSMode read')

    value=np.array(range(number), dtype=np.float)
    for i in range(number):
        PM.write(':AVER 10' )
        PM.write('CORR:WAV '+str(WL))
        value[i]=float(PM.query('READ?'))

    ## calculate mean and standard deviation
    avrg_power=np.mean(value)
    std_power=np.std(value)

    ## calculate uncertainty
    if WL<440 and WL>=280:
        unc=np.sqrt(std_power**2+(avrg_power*0.05)**2)
    elif WL>=440 and WL<981:
        unc=np.sqrt(std_power**2+(avrg_power*0.03)**2)
    elif WL>=981 and WL<1101:
        unc=np.sqrt(std_power**2+(avrg_power*0.07)**2)
    elif WL>=200 and WL<280:
        unc=np.sqrt(std_power**2+(avrg_power*0.07)**2)

    return avrg_power,unc,Zeit
```

B.2 Measuring the Current

Opening the pA-Meter: `openKeithley.py`

Again, it is necessary to open the pA-meter as an object inside python:

```
# -*- coding: utf-8 -*-
"""
Created on Tue Aug  2 14:11:42 2016

@author: pcalab
"""
def openKeithley(rm,time):
    ## open Keithley via the right socket
    Keith = rm.open_resource(\
    'TCPIP::134.30.30.48::4005::SOCKET')
    print(Keith)
    ## Keithley has no hardware handshake, end read on LF
    Keith.read_termination = Keith.LF
    ## Return 6487 to RST defaults
    Keith.write('*RST')
    time.sleep(.1)
    ## print ID number
    print(Keith.query('*IDN?'))
    ## Select reading and timestamp
    Keith.write('FORM:ELEM READ')
    time.sleep(.1)
    ## Enable autorange
    Keith.write('SENS:RANG:AUTO 1')
    time.sleep(.1)
    ## set bias voltage
    Keith.write('SOUR:VOLT:RANG 500')
    time.sleep(.1)
    try:
        biasV=int(input("Wert der Vorspannung?\
        \n Standard: 300V \n Ihre Eingabe:"))
    except:
        biasV=300

    Keith.write('SOUR:VOLT '+str(biasV))
    time.sleep(.1)
    Keith.write('SOUR:VOLT:ILIM 2.5e-3')
    time.sleep(.1)
    Keith.write('SOUR:VOLT:STAT ON')
    time.sleep(.1)
    ## Disable zero check
    Keith.write('SYST:ZCH OFF')

    return Keith, biasV
```

Measuring the Spectral Current: `Strom.py`

As for the measurement of the spectral power, the monochromator motor is triggered in a certain wavelength region, devided into a certain stepsize in order to measure the spectral current:

```
# -*- coding: utf-8 -*-
"""
Created on Thu Aug  4 13:49:43 2016

@author: pcalab
"""
## import modules
import numpy as np
import time
import Keithley_Meas
import matplotlib.pyplot as plt

def Strom(Keith,WL,Bereich1,Bereich2,DefBer,\
            WrtBer,Std,Zeit,Steps,f,Mono):
    ## moving motor to dedicated range and steps
    for i in range(len(DefBer)):
        print(Bereich1+i*Steps)
        Distance2=((Bereich1-WL)+i*Steps)*f
        move2="X" +str(Distance2) +"g"
        Mono.write(move2)
        time.sleep(3)
        ## current measurement
        WrtBer[i],Std[i],Zeit[i]=\
        Keithley_Meas.Keithley_Meas(Keith)
        time.sleep(1)

        ## ploting the measured data
        #fig=plt.figure()
        plt.scatter(DefBer[0:i+1],WrtBer[0:i+1])
        plt.axis([Bereich1, Bereich2,min(WrtBer[0:i+1]),\
                  max(WrtBer[0:i+1])])
        plt.show()

    ## dark current
    I_D=np.array(range(1),dtype=np.float)
    Unc_ID=np.array(range(1),dtype=np.float)
    Zeit_ID=np.array(range(1),dtype=np.float)

    input('I_D messen; Lichtstrahl entfernen!\
           Enter, um zu messen')
    I_D[0],Unc_ID[0],Zeit_ID[0]=\
    Keithley_Meas.Keithley_Meas(Keith)
    I_dark=I_D,Unc_ID,Zeit_ID
    ## substract the dark current
```

```
45      WrtBer=abs(WrtBer)-abs(I_D)
46      plt.scatter(DefBer,WrtBer)
47      Std=np.sqrt(Std*Std+Unc_ID*Unc_ID)
48
49      fig=plt.figure()
50      plt.scatter(DefBer[0:i+1],WrtBer[0:i+1])
51      plt.axis([Bereich1, Bereich2,min(WrtBer[0:i+1]),\
52                  max(WrtBer[0:i+1])])
53
54      I_cont=DefBer,WrtBer,Std,Zeit
55
56      return I_cont, I_dark, fig
```

A Single Current Measurement: `Keithley_Meas.py`

The current is measured for each wavelength step:

```
1  # -*- coding: utf-8 -*-
2  """
3  Created on Thu Aug  4 13:49:43 2016
4
5  @author: pcalab
6  """
7  ## import modules
8  import time
9  import numpy as np
10
11 def Keithley_Meas(Keith):
12      ## record time
13      Zeit=time.strftime("%Y%m%d%H%M%S")
14      ## do 20 measurements
15      ## set trigger model to 20 readings
16      Keith.write('TRIG:COUN 20')
17      time.sleep(0.1)
18      ## set buffer size to 20
19      Keith.write('TRAC:POIN 20')
20      time.sleep(0.1)
21      ## store raw input readings
22      Keith.write('TRAC:FEED SENS')
23      time.sleep(0.1)
24      ## start storing readings
25      Keith.write('TRAC:FEED:CONT NEXT')
26
27      ## trigger readings setup to SRQ on
28      Keith.write('INIT')
29      time.sleep(0.1)
30      ## Request all stored readings
31      # Keith.query('TRAC:DATA?')
32      # time.sleep(0.1)
```

```
33      ## read all stored readings; not saved because
34      ## mean value is more interesting
35      # Keith.read()
36
37      time.sleep(0.1)
38
39      ## acquire mean statistic for buffer readings
40      ## trigger readings setup to SRQ on
41      Keith.write('CALC3:FORM MEAN')
42      ## time depends on the number of readings
43      ## 5s -> 20 readings
44      time.sleep(5)
45      #Keith.wait_for_srq()
46      ## request all stored readings
47      mean_curr_num=float(Keith.query('CALC3:DATA?'))
48      # mean_curr_num=Keith.read()
49      print(mean_curr_num)
50      time.sleep(0.1)
51      ## select mean statistic
52      Keith.write('CALC3:FORM SDEV')
53      time.sleep(0.1)
54      ## request mean statistic
55      std_curr_num=float(Keith.query('CALC3:DATA?'))
56      # std_curr_num=Keith.read()
57
58      ## calculate accuracy
59      if np.abs(mean_curr_num) <= 2e-9:
60          acc=0.003*mean_curr_num+400e-15 ## fA
61      elif np.abs(mean_curr_num) <= 20e-9:
62          acc=0.002*mean_curr_num+1e-12 ## pA
63      elif np.abs(mean_curr_num) <= 200e-9:
64          acc=0.0015*mean_curr_num+10e-12 ## pA
65      elif np.abs(mean_curr_num) <= 2e-6:
66          acc=0.0015*mean_curr_num+100e-12 ## pA
67      elif np.abs(mean_curr_num) <= 20e-6:
68          acc=0.001*mean_curr_num+1e-9 ## nA
69      elif np.abs(mean_curr_num) <= 200e-6:
70          acc=0.001*mean_curr_num+10e-9 ## nA
71      elif np.abs(mean_curr_num) <= 2e-3:
72          acc=0.001*mean_curr_num+100e-9 ## nA
73      elif np.abs(mean_curr_num) <= 20e-3:
74          acc=0.001*mean_curr_num+1e-6 ## muA
75
76      ## uncertainty
77      unc=np.sqrt(std_curr_num**2+acc**2);
78      print(unc)
79
80      return mean_curr_num,unc,Zeit
```

B.3 The Main Program: `IorP.py`

Using the main program uses the aforementioned programms to either measure the spectral current or the spectral power:

```
1  # -*- coding: utf-8 -*-
2  """
3  Created on Tue Aug  2 11:29:26 2016
4
5  @author: pcalab
6  """
7  ## import modules
8  import visa
9  import numpy as np
10 import time
11 import openPM
12 import openKeithley
13 import Leistung
14 import Strom
15 import os
16
17 ##------------------------------------------------
18 rm=visa.ResourceManager()
19
20 ## choose measurement
21 Messung=input("Strom(I) oder Leistung(P) messen?")
22
23 strom='I'
24 leistung='P'
25
26 if Messung==strom or Messung==leistung:
27     print('Gemessen wird '+Messung)
28 else:
29     print('falsche Eingabe\n')
30
31 ## main program
32 ##------------------------------------------------
33 try:
34     ## open instruments
35     ## open keithley
36     if Messung==strom:
37         Keith,biasV=openKeithley.openKeithley(rm,time)
38     ## open monochromator motor
39     Mono=rm.open_resource('ASRL3::INSTR')
40     print(Mono)
41     ## open power meter
42     PM,minBer,maxBer=openPM.openPM(visa)
43     ##-----------------------------------------
44     ## initialize monochromator motor
```

```
45      ## steppermotor steps per nm
46      f=32
47      ## go to 0(initialize)
48      Mono.write('X000g')
49      WL=int(input("Wo bin ich?"))
50      ##-----------------------------------------
51      ## ask for slitwidths
52      try:
53          strSlit='Schlitzweite? \n Standard: (1mm 1mm)\
54                                   \n Ihre Eingabe:'
55          Slitwidth1,Slitwidth2=input(strSlit).split()
56          Slitwidth1,Slitwidth2=\
57          [int(Slitwidth1),int(Slitwidth2)]
58      except:
59          Slitwidth1,Slitwidth2=1, 1
60      # print(Slitwidth1, Slitwidth2)
61      ##-----------------------------------------
62      ## ask for scanning range
63      strBer='Welchen Bereich (min='+str(minBer)+\
64      ' max='+str(maxBer)+') messen?\
65      \n Standard: (370 700)\
66      \n Ihre Eingabe:'
67
68      try:
69          Bereich1, Bereich2 = input(strBer).split()
70          Bereich1, Bereich2 = [int(Bereich1), int(Bereich2)
71          if Bereich1>Bereich2:
72              print("Bitte von klein nach gross schreiben")
73          elif Bereich1<minBer or Bereich2>maxBer:
74              print("Liegt nicht im Messbereich der Diode")
75      except:
76          Bereich1, Bereich2=370, 700
77      # print(Bereich1, Bereich2)
78      ##-----------------------------------------
79      ## ask for stepsize
80      try:
81          strSteps='Abstand(nm)? \n Standard: 5\
82                                   \n Ihre Eingabe:'
83          Steps=int(input(strSteps))
84      except:
85          Steps=5
86      ##-----------------------------------------
87      ## does the stepsize fit with the  scanning range?
88      a=np.mod(Bereich2-Bereich1,Steps)
89      if a!=0:
90          print("Ist kein Teiler")
91      else:
92          ## start time measurement
93          tic=time.time()
```

```
94
95          ## generate arrays
96          length=int((Bereich2-Bereich1)/Steps+1)
97
98          DefBer=\
99          np.array(range(Bereich1, Bereich2+Steps, Steps))
100         WrtBer=np.array(range(length),dtype=np.float)
101         Std=np.array(range(length),dtype=np.float)
102         Zeit=np.array(range(length),dtype=np.float)
103         ## go to lower scanning limit
104         time.sleep(3)
105         Distance1=(Bereich1-WL)*f
106         move1='X'+str(Distance1)+'g'
107         Mono.write(move1)
108         # time.sleep(10)
109
110         ## start measurement
111         ## power
112         if Messung==leistung:
113             P_cont,Mono,fig=Leistung.Leistung(PM,WL,\
114             Bereich1,Bereich2,DefBer,WrtBer,Std,\
115             Zeit,Steps,f,Mono)
116             np.savetxt('P_cont.txt',np.c_[P_cont],\
117             fmt='%.18g',delimiter=' ', newline=os.linesep)
118         ## current and dark current
119         elif Messung==strom:
120             I_cont,I_dark,fig=Strom.Strom(Keith,WL,\
121             Bereich1,Bereich2,DefBer,WrtBer,Std,\
122             Zeit,Steps,f,Mono)
123             np.savetxt('I_cont.txt',np.c_[I_cont],\
124             fmt='%.18g', delimiter=' ',newline=os.linesep)
125             np.savetxt('I_dark.txt',np.c_[I_dark],\
126             fmt='%.18g', delimiter=' ',newline=os.linesep)
127         ## nothing was chosen
128         else:
129             print("Keine Messung ausgewaehlt")
130         ## stop time measurement
131         toc=time.time()-tic
132     ## save current figure to pdf and png
133     fig.savefig("contMeas.pdf")
134     fig.savefig('contMeas.png',dpi=600)
135     ##-----------------------------------------
136
137 ## close devices
138 finally:
139
140     ## close keithley
141     if Messung==strom:
142
```

```
143             Keith.write('SOUR:VOLT:STAT OFF')
144             time.sleep(.1)
145             Keith.write('SYST:ZCH ON')
146             Keith.close()
147         ## save additional information
148             ## save slithwidths, stepsize and bias voltage
149         if Messung==strom:
150             ZusatzinfoI=Slitwidth1, Slitwidth2, Steps, biasV
151             np.savetxt('Zusatzinfo.txt',np.c_[ZusatzinfoI],\
152             fmt='%.18g',delimiter=' ', newline=os.linesep)
153             ## save slithwidths and stepsize
154         else:
155             ZusatzinfoP=Slitwidth1, Slitwidth2, Steps
156             np.savetxt('Zusatzinfo.txt',np.c_[ZusatzinfoP],\
157             fmt='%.18g',delimiter=' ', newline=os.linesep)
158         ## close Mono
159         Mono.close()
160         ## close Power Meter
161         PM.close()
162 ## don't forget to save figures and data under a new name!
163 input('Variablen und Bilder speichern!\
164               bel. Taste druecken')
```

References

1. Bilderback, D. H., Elleaume, P. & Weckert, E. Review of Third and Next Generation Synchrotron Light Sources. *Journal of Physics B: Atomic, Molecular and Optical Physics* **38,** 773–797 (2005).
2. Abo-Bakr, M. *et al.* Status of the HZB ERL Project bERLinPro. *Proceedings of IPAC2014, Dresden, Germany* (2014).
3. HZB. *3D-Ansicht bERLinPro - ERL Gesamt* `http://wiki.trs.bessy.de/bin/view/BERLinPro/BerlinProWarmSystems`. [accessed July–2016]. 2016.
4. Schmeisser, M. *In-situ measurements of the intrinsic emittance of photocathodes for high brightness electron beams* Master's Thesis (Humboldt-Universität Berlin, 2014.).
5. Spicer, W. E. Photoemissive, Photoconductive, and Optical Absorption Studies of Alkali-Antimony Compounds. *Phys. Rev.* **112,** 114 (1958).
6. Dunham, B. *et al.* Record High-Average current from a High-Brightness Photoinjector. *Applied Physics Letter* **102,** 034105 (2013).
7. Spicer, W. E. & Herrera-Gomez, A. Modern Theory and Applications of Photocathodes. *SPIE's 1993 Interantional Symposium on Optics, Imaging and Instrumentation* (1993).
8. Gosh, C. & Varma, B. P. Preparation and Study of properties of a few Alkali Antimonide Photocathodes. *Journal of Applied Physics* **49,** 4549–4553 (1978).
9. Lederer, S. *et al.* Photocathodes at Flash. *Proceedings of FEL2011, Shanghai, China.* `https://accelconf.web.cern.ch/accelconf/FEL2011/papers/thpa19.pdf` (2011).
10. Dowell, D. H. *et al.* In situ cleaning of metal cathodes using a hydrogen ion beam. *Phys. Rev. Special Topics - Acc. and Beams* **9** (2006).
11. *An Engineering Guide to Photoinjectors* (eds Rao, T. & Dowell, D. H.) ISBN: 1481943227 (Triveni Rao, David H. Dowell, 2013).
12. DESY. *FLASH - Free-Electron Laser* `https://flash.desy.de/`. [accessed November–2016]. 2016.
13. Kirschner, H. *Spectral Quantum Efficiency Measurements on CsK_2Sb photocathodes for bERLinPro* Forschungsbeleg (Humboldt-Universität Berlin, 2016.).
14. HORIBA. *Lamp Power Supply Operation Manual* Optical Building Blocks Corporation (Birmingham, New Jersey, USA, 2007.).
15. HORIBA. *PowerArc Broadband Arc Lamp Housing and Power Supply* `http://www.obbcorp.com/optical-components/light-sources/broadband-illuminators/arc-lamp-housings/PowerArc/index.html`. [accessed June–2016]. 2016.
16. HORIBA. *Monochromator Operation Manual* Optical Building Blocks Corporation (Edison, New Jersey, USA, 2007–2015.).
17. HORIBA. *Xenon Arc Lamp Spectrum* `http://www.obbcorp.com/optical-components/light-sources/broadband-illuminators/arc-lamp-housings/PowerArc/PowerArc-Specifications.html`. [accessed June–2016]. 2016.

18. Thorlabs. *Power Meter Bundle PM130D* http://www.thorlabs.de/newgrouppage9.cfm?objectgroup_id=4216. [accessed June–2016]. 2016.

19. Thorlabs. *Photodiode Power Sensors(C-Series)* http://www.thorlabs.de/newgrouppage9.cfm?objectgroup_id=3328. [accessed June–2016]. 2016.

20. Tektronix. *Datasheet for Keithley 6485* http://www.tek.com/sites/tek.com/files/media/media/resources/6485.pdf. [accessed July–2016]. 2016.

21. VACOM. *CF-viewport, DN16* www.vacom-shop.de/VPCF16B-L/en. [accessed July–2016]. 2016.

22. Reiser, M. *Theory and Design of Charged Particle Beams* Wiley Series in Beam Physics and Accelerator Technology (Wiley-VCH Verlag GmbH & Co. KGaA, 2008).

23. Newport. *Colored-Glass Alternative Filter, 400 nm Longwave Pass Cut-on* https://www.newport.com/p/20CGA-345. [accessed June–2016]. 2016.

24. Thorlabs. *Iris diameter* https://www.thorlabs.de/newgrouppage9.cfm?objectgroup_id=220. [accessed August–2016]. 2016.

25. Sommer, A. H. *Photoemissive Materials* ISBN: 471813001 (John Wiley & Sons, Inc., New York, USA, 1968).

26. Feng, J. *et al. Near atomically smooth alkali antimonide photocathode thin films* https://arxiv.org/abs/1610.04288. 2016.

27. Moulder, J. F. *et al. Handbook of X-ray Photoelectron Spectroscopy* Wiley Series in Beam Physics and Accelerator Technology. ISBN: 0-9648124-1-X (Physical Electronics, Inc., Eden Prairie, Minnesota, USA, 1995).

28. Kong, S. H. *et al.* Photocathodes for free electron lasers. *Nuclear Instr. and Methodes in Physics Research* **358,** 272–275 (1995).

29. Seimiya, Y. *CsKSb Photocathode R&D with High Quantum Efficiency and Long Lifetime* in *Proceedings of IPAC2015* (2015.).

30. Mamun, M. A. *et al.* Correlation of CsK_2Sb photocathodes lifetime with antimony thickness. *APL Materials* **3,** 066103 (2015).

31. Nathan, R. & Mee, C. H. B. The Preparation of Potassium–Antimony–Caesium Photocathodes. *Journal of Physics* **1,** 351 (1968).

32. Xie, H. *et al.* Experimental measurements and theoretical model of the cryogenic performance of bialkali photocathode and characterization with Monte Carlo simulation. *Physical Review Accelerators And Beams* **19** (2016).

33. Nathan, R. & Mee, C. H. B. Photoelectric and Related Properties of the Potassium–Antimony–Caesium Photocathode. *Int. J. of Electronics* **23,** 349–354 (Oct. 1967).

34. Konomi, T. *et al. Record Performance of SRF Gun with CsK_2Sb Photocathode* in *Proceedings of SRF2015* (2015.).

35. Kane, E. O. Theory of Photoelectric Emission from Semiconductors. *Phys. Rev.* **127,** 131 (1962).

Acknowledgements

First, I would like to acknowledge Prof. Andreas Jankowiak, for giving me the opportunity to write my master thesis at the HZB. Also great thanks to Dr. Thorsten Kamps, who received me kindly in his working group, which I like to thank as well for the nice cooperation and the pleasant lunches during my time there.

I greatly appreciated the help of Dr. Guido Klemz, who supported me with calm and well-grounded knowledge.

Especially I am indebted to Dr. Julius Kühn and Martin Schmeißer for their teamwork at the cathode lab and their continous support on my scientific work as well as on the presentation of my results, like this master thesis.

On this occasion I also like to say thanks to Markus Bürger for the engineering support.

Zum Schluss möchte ich gerne meinen Eltern danken, für die jahrelange Unterstützung, nicht nur während meines Studiums, sondern auch in allen anderen Lebenslagen. Danke.

Selbständigkeitserklärung

Hiermit versichere ich, dass ich die vorliegende Arbeit selbstständig verfasst, keine anderen als die angegbenen Quellen und Hilfsmittel verwendet habe und erstmalig eine Masterarbeit einreiche. Die Bearbeitung erfolgte unter Beachtung der gültigen Prüfungsordnung.

Berlin, den 7. Januar 2017